EXPLORATORY STUDY OF GOLD NANOSHELL AS A THERAPEUTIC THERMAL ABLATION AGENT FOR CANCER TREATMENT USING LABORATORY AND ANIMAL TISSUE PHANTOMS

by

YAJUVENDRA RATHORE

Presented to the Faculty of the Graduate School of

The University of Texas at Arlington in Partial Fulfillment

of the Requirements

for the Degree of

MASTER OF SCIENCE IN BIOMEDICAL ENGINEERING

THE UNIVERSITY OF TEXAS AT ARLINGTON

December 2009

ACKNOWLEDGEMENTS

At the outset, I would like to express my sincere gratitude to all the people who helped me make this thesis possible.

It is difficult to overstate my gratitude to my supervisor, Dr. Hanli Liu. She gave inspiration throughout my work and guided and supported me in all the possible ways. During the course of the research, she provided me encouragement, sound advice, good teaching and many ideas to make my thesis better. Without her valuable suggestions, support and guidance this thesis would not have been possible.

I owe my most sincere gratitude to Dr. George Alexandrakis for guiding me throughout the course of my thesis. I would also like to thank him for teaching courses on tissue optics and fluorescence microscopy which made the foundation for my thesis.

I thank Dr. Liping Tang and Dr. Jinhui Shen for their help and support during the entire course of this project. I also express my thanks to Dr. Kytai Nyugen for accepting my request to be a committee member.

I thank my friends Nimit, Sweta and Zi-Jing for their valuable advice, friendly help and encouraging words. Lastly and most importantly, I wish to thank my parents, Lalita and Liladhar Rathore and my family who raised, supported, taught, loved and inspired me to earn things through hard work and sincerity. To them I dedicate this thesis.

November 18, 2009

ABSTRACT

EXPLORATORY STUDY OF GOLD NANOSHELL AS A THERAPEUTIC THERMAL ABLATION AGENT FOR CANCER TREATMENT USING LABORATORY AND ANIMAL TISSUE PHANTOMS

Yajuvendra Rathore, M.S.

The University of Texas at Arlington, 2009

Supervising Professor: Dr. Hanli Liu

Prostate cancer is the most common male cancer in the United States and the second leading cause of male death from cancer. Surgical removal of the prostate is associated with high risks of surgical complications and consequences such as incontinence and sexual dysfunction. In my study, I have investigated a nanoparticle-assisted photothermal therapeutic method that may be used for treatment of prostate cancer in the future. This method is minimally-invasive and uses gold nano-shells as hyperthermia agents to treat localized necrosis of cancer cells.

I have conducted a feasibility study for a new class of NIR absorbing nanoparticles called Gold Nanoshells for interstitial laser-induced thermal therapy. These are optically tunable nanoparticles, consisting of a dielectric core (silica) coated with an ultrathin metallic layer (gold). These metal coated nanoshells were utilized to convert the absorbed near-infrared light to heat with more efficacy and stability. Extensive study was performed on tissue simulating phantoms in order to examine the temperature profiles. With different concentrations of gold nanoshells, temperature profiles as a function of distance (mm) from the spot of illumination were determined. The phantom study was also aimed to determine the optimal power, concentration of gold nanoshells, and heat spread over vicinity. The results of phantom study were then used to carry out animal tissue study, where direct injections of gold nanoshell suspensions into chicken tissue were performed and rapid heating of gold nanoshell embedded tissues upon exposure to the near infrared light was measured. This procedure will provide the relationship among nanoshell dosages, light intensity, and duration of illumination for tissue damage. The success of this project will be helpful in exploring new treatment techniques (i.e., hyperthermia) for prostate cancer, thus improving the quality of life for prostate cancer patients. Furthermore, this technology can also be applicable to other types of solid tumors/cancers for improved therapeutic outcome.

TABLE OF CONTENTS

LIST OF ILLUSTRATIONS

LIST OF TABLES

CHAPTER 1

INTRODUCTION

1.1 Prostate

A normal-sized prostate is a small walnut sized exocrine gland of the male reproductive system. It is located between the bladder and the penis, anterior to the rectum, and above the sphincter & the penis. Prostate gland in men, similar to breast in woman, is to store and produce seminal fluid. It is muscular and glandular, with ducts are lined by transitional epithelium [1, 2]. This ducts open into the prostatic portion of the urethra which runs through the center of the prostate, from the bladder to the penis, and allow urine to flow out of the body [3].

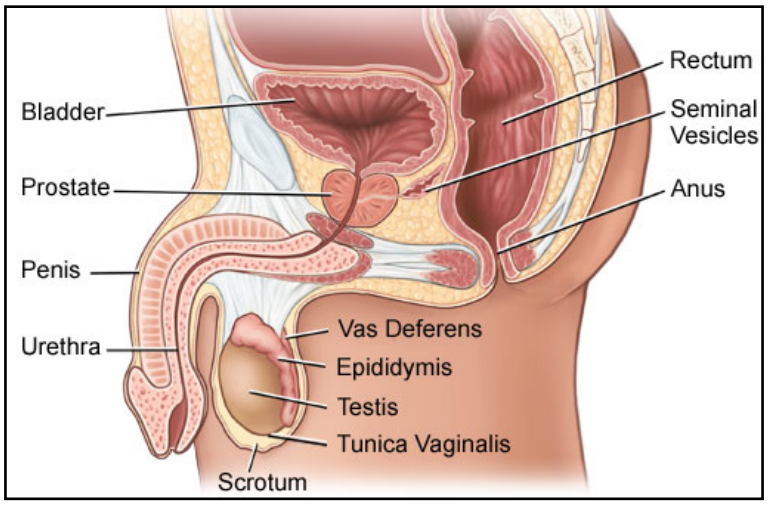

Figure 1.1 Male Reproductive Tract [4].

As part of the male reproductive system, the primary function of the prostate is to secrete a slightly alkaline fluid which constitutes about 10-30% of the seminal fluid. During ejaculation, alkaline fluid activates the sperms and squeezes into the urethra, by prostate. It is then expelled with sperm as semen. The acidity of the vaginal tract is neutralized by alkaline liquid which helps to prolong the lifespan of the sperm. The urethra passes through the center of the prostate and merges with the ejaculatory ducts (the male urethra has two functions). The gland is enclosed on the pelvic floor muscles which contract during ejaculation. It consists of three lobes: a center lobe with one lobe on each side. It can be divided into four distinct zones, characterized by differing embryological origin, location and pathologies [4, 5, 7].

Peripheral Zone: This zone is the sub-capsular portion of the prostate gland which surrounds the urethra. In this zone, glands are normally small and simple but the main site of origin for prostate cancer is about 70%.

Central Zone (CZ): Central zone surrounds the ejaculatory ducts and constitutes approximately about 25% of the prostate cancer origin.

Transition Zone (TZ): This zone region surrounds the proximal urethra and also responsible for benign prostatic hypertrophy. However, this zone only accounts 5% chance for the origin of cancer. Also, this is the region of the prostate gland which grows throughout life.

Anterior fibro-muscular Zone: This zone is only consists of muscles and the fibrous tissue with very few glandular components.

1.1.1 Growth of a prostate

At birth, the size of prostate gland is very small and remains same throughout early childhood. During puberty, stages marked by body in addition to hormone changes, the growth of the prostate occurs due to induced testosterone which is the male sex hormone. However, the prostate continues to grow due to the enlargements of glands as well as due to the muscle present within the prostate. This enlargement of the prostate gland with age is called Benign Prostatic Hypertrophy (BPH). Furthermore, the BPH is not related with cancer, but it is a problem which requires treatment. In general, the prostate cancer occurs in older men and nearly 60% of the male population.

1.1.2 Prostate cancer

Prostate cancer is one of the most common types of cancer in men. Prostate cancer is a type of cancer which grows in prostate gland in males that produces seminal fluid. It involves in the growth of abnormal cells usually in the peripheral zone, and particularly close to the outer surface of the prostate. Initially, prostate tumors do not show urinary symptoms because it does not put pressure on the urethra. It usually grows slowly and initially spread to the interior of the gland, which may not be serious. However, there are some types of prostate cancer which are aggressive and can spread quickly. At early stage, in which it grows slowly may require minimal or no treatment and have a better chance of successful treatment. Various symptoms are seen during this stage: pain, difficulty in urinating, problems during sexual intercourse, and erectile dysfunction. It is grouped on the basis of tumor size, spreading, and different tumor cells. This is known as staging, it may help the doctor to determine which treatment is

suitable. Prostate cancer may spread to tissues near the prostate and as well as to distant parts of the body. Prostate cancers which are limited to the gland are often treated successfully [6].

1.2 Prostate cancer diagnosis

For prostate cancer detection, doctors follow up an elevated PSA (Prostate Specific Antigen) or positive DRE (Digital Rectal Examination) with more definitive testing. Some physicians employ Trans-rectal ultrasound (TRUS), which uses a rectal probe that creates a video image of the prostate using harmless sound waves collected by a computer. TRUS helps the physician decide if a biopsy is needed. If biopsy is needed, the doctor will take tiny prostate tissue samples with a small-gauge needle, injected typically through the rectum. A pathologist then examines the samples under a microscope after the prostate samples are collected. Once cancer is diagnosed, other tests such as computerized tomography, lymph-node biopsies, and bone scans can be used to determine if tumors have spread beyond the prostate [6].

1.3 Treatment Modalities

Various treatment techniques have been employed to treat prostate cancer after examination of elevated prostate specific antigen or positive digital rectal examination. At present, most widely used treatment techniques involves prostatectomy, radiation therapy, chemotherapy, cryotherapy, and hormone therapy (figure 1.2).

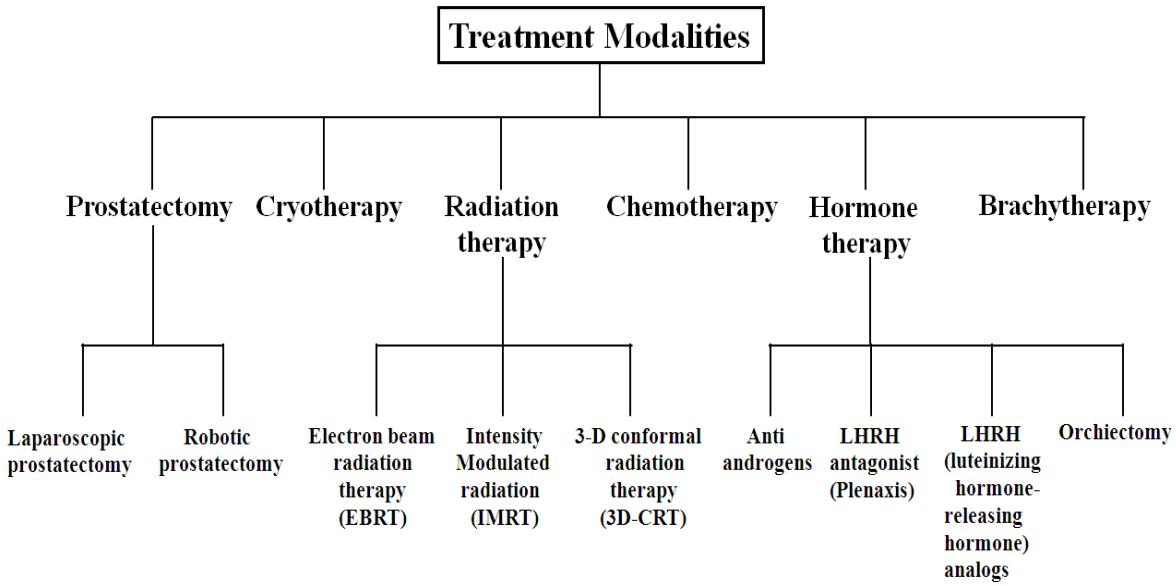

Figure 1.2 Classification of treatment modalities for prostate cancer treatment.

In Prostatectomy, treatment can be carried out by a single incision or by a series of small incisions to the lower abdomen or perineum. This technique is one of the oldest prostate cancer treatment techniques. However, it is employed invasively by which prostate and seminal vesicles are removed to prevent cancer. Small incisions are placed on the abdomens to permit the instruments and the video camera to pass through. This procedure employs video camera to help surgeon to observe the surgery. Prostatectomy technique can be classified as: laparoscopic prostatectomy and robotic prostatectomy.

Both are the two latest surgical techniques for prostate cancer treatment which can be performed using one of the two ways: extraperitoneal and transperitoneal. A thin membrane which lines the abdominal cavity and envelops most of the abdominal organs is peritoneum. In extraperitoneal prostatectomy, it is required to cut through peritoneum membrane, whereas it is not required in the transperitoneal prostatectomy. Also, in some cases longer recovery times and more complications for patients are observed, undergone the transperitoneal prostatectomy. The major drawbacks associated with prostatectomy are surgical risks as it is performed invasively and deep venous thrombosis, which arises after blood travels very slowly through the veins in the legs and starts to clot. However, there are risks for pulmonary embolism, heart attack, or stroke cause due to lodging of clot, which breaks off and travels through the body, in the lungs, heart, or brain. In addition, there is a risk of infection associated with patient at the location of the incision or at the exit of the catheter from the penis. The most frequently observed side effects after radical prostatectomy are impotence and incontinence [8].

Cryotherapy, also known as cryosurgery and cryoablation is one of the new prostate cancer treatment techniques. In cryotherapy, the main aim is to destroy prostate cancer by freezing or using thaw cycles. It is also invasive surgery in which after receiving anesthesia, the physician introduces needles into the prostate gland through the perineum, the area between the scrotum and anus. These needles generate very cold temperatures and help to destroy the entire prostate, together with cancerous tissue. In

some cases it is useful to employ freezing temperatures rather than stronger doses of radiation therapy for prostate cancer treatment. However, there are some disadvantages associated with this technique like it lacks long term survival studies, risk of impotency, and risk of side effects which include moderate pelvic pain, blood in the urine, mild urinary urgency, scrotal swelling [8].

Radiation therapy is the most common technique used for prostate cancer treatment. It oldest type is electron beam, whereas intensity modulated, 3D-CRT, and proton beam therapy come under newer versions. In principle, this technique employs high-energy rays to kill cancer cells, which are limited within prostate gland. However, in cancers which are limited to prostate gland, results are much similar to those patients for getting prostatectomy. Radiation therapy is categorized into two groups: external beam radiation and internal beam radiation (brachytherapy). The main goal of treatment is to damage the DNA of cells using high energy radiation, which can destroy cancer cells. An appropriate amount and aimed energy will be required for destruction of cancer cells, since cancerous tissue divide more rapidly compare to healthy tissue. The most commonly used radiation therapies are the conventional electron beam radiation therapy (EBRT), 3D-conformal radiation therapy and intensity modulated radiation (IMRT). All the three types of radiation therapy employ same type of particle called photons, which have no electric charge and no rest mass. Furthermore, there are some disadvantages associated with radiation therapy which causes risk to patient health. These risks occur due to variety of side effects, since healthy tissue are often destroyed

together with the targeted cancer cells. These risks involve bladder problem, urinary incontinence, impotence, tiredness, lymphedema, skin reactions in treated areas, diarrhea, and rectal irritation and bleeding. There may be risk of permanent side effects like bowel function may not be normal even after treatment [8].

Chemotherapy is performed using different drugs in order to treat cancerous cells. This therapy is not mainly use for cancer which is limited to prostate, but it usually employed for cancer extended outside of the prostate gland. It is also used in combination with other therapies with the aim of treating cancerous cells. It aid in reducing pain and tumor growth and therefore, it is usually use as salvage therapy. On the other hand, drugs employed in chemotherapy are toxic and systemic. These drugs destroy cells in such a way that upon division the cell dies and that is why they are toxic. While, this therapy has systemic affects as it travels through the blood stream affecting other cells of the body. Furthermore, it is not focused to any particular area of the body and lacks localized treatment alternative. Therefore, cells which divide rapidly which include follicles, skin, gastrointestinal tract, and bone marrow are mostly affected. Benefits of chemotherapy for early prostate cancer treatment are overshadowed by the side effects of chemotherapy drugs [8].

This therapy targets systemic ablation of the male hormones, which helps to prevent the growth of prostate cancer. This therapy is also known as androgen deprivation ablation therapy. The main aim is to decrease the levels of androgens, hormones in the male body. Testosterone and dihydrotestosterone are the two main

androgens in the male body. These hormones are mainly secreted in the testicles and helps in prostate cancer cells growth. Decreasing androgen levels usually helps to shrink prostate cancer and also prevents prostate cancer growth. On the other hand, this therapy does not cure prostate cancer patient from cancer. There are many side effects associated with hormone therapy which includes impotency, hot flashes, osteoporosis, anemia, breast tenderness and growth of breast tissue, decreased mental acuity, weight gain, fatigue, increased cholesterol, depression [9].

One more type of radiation therapy used for prostate cancer treatment known as Brachytherapy. This therapy is also called as interstitial radiation therapy, seed therapy. In this therapy, high and concentrated doses of radiation are employed for the treatment. Side effects associated with Brachytherapy include feelings of urgency, frequent urination, and also with slower and weaker urinary streams. Sexual side effects are also common [9].

1.4 Motivation for research

In medical field, application of locally induced hyperthermia proved to be promising as a treatment tool for different cancers. In this methodology, irreversible tissue damage, which is due to loosening of cell membranes and denatured proteins, is caused by means of heat [10]. Hyperthermia induced cancer treatment through heat sources like focused ultrasound waves, radio waves and near infrared (NIR) lasers has been investigated in animal models for past few years [11, 12]. Unfortunately, these simple heating techniques have some limitations due to complexity in controlling delivering heat dosage and restricting the effects to the tumors. This leads to ablation of healthy tissue too, which destroys healthy tissue along with cancerous tissue in the process of treatment. However, these limitations are overcome by the application of laser light through thin optical fibers. Laser energy in most cases delivered interstitially to tumors through fibers into the center of the tumor area [13]. The major disadvantage using laser is very high laser power output is required to effectively treat cancerous part. In alternative techniques, which employ photosensitizing drugs and photothermal agents to absorb light, demonstrate effective way to lower down the higher laser power for tissue ablation. Due to drawbacks associated with drugs and dyes, which are toxic in nature and are not biocompatible, limits the application of these techniques [12].

As currently available treatment modalities have drawbacks, there is a growing demand to develop a safe, cost and time effective treatment technique. In the past few years, near infrared (NIR) light has been employed both in imaging and treatment technique for prostate cancer. Light incident on tissue undergoes multiple scattering

and absorption. Figure 1.3 shows the absorption spectra of various chromophores in the tissue in NIR wavelength range (700-900 nm). NIR photons are absorbed less by the tissue chromophores as compared to visible photons [14], which in turn results in greater penetration in tissue by the NIR photons. Therefore, light penetration through tissue is optimal in the NIR 'tissue window'. Recently, laser activated gold nanoshell thermal ablation technique for cancer treatment has been studied by various groups [12-15]. In this technique, optically tunable nanoparticles consist of core coated with an ultra thin gold layer acts as a photo-sensitizer and helps in depositing heat in the targeted tissue to cause photothermal reactions [11,12]. However, detailed study of heat spread as a function of excitation energy requires further investigation. I proposed a novel approach of administrating gold nanoshell to the tumor site via local injection. Successful implementation of this approach could reduce patient dosage of nanoshells and minimize healthy tissue damage significantly, as compared to the earlier approach of intravenous injection and simple heat source.

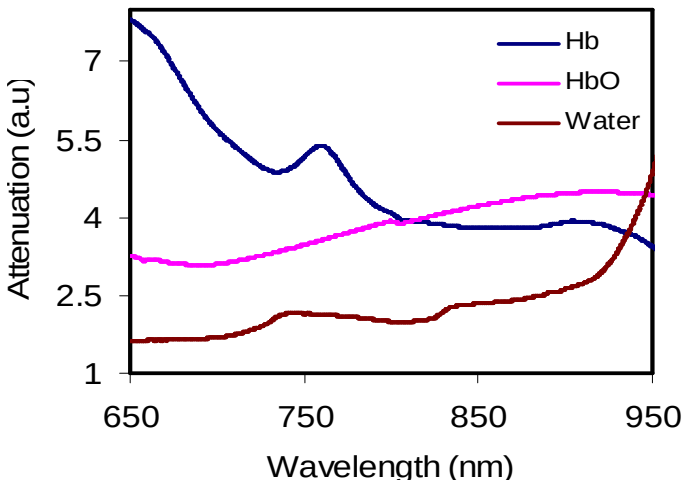

Figure 1.3 Absorption characteristics of tissue chromophores in the near infrared wavelength region.

CHAPTER 2

GOLDNANOSHELL AND ITS APPLICATION

2.1 Introduction

In recent years, new medical technologies employ gold as a new tool in fighting cancer. Emerging nanotechnology has offered development of a new class of nanoparticles called Gold nanoshells. In improving biomedical solutions, these uniquely designed gold nanoshells played a key role because of their properties and characteristics which involves nanoscale size, optical tunability, and chemical stability. Nanoshells are being examined and are appears to be promising, both for imaging and treatment of cancer. Nanoshells can be administered to targeted cancer cells and their properties can be altered for particular application. In addition, gold being a noble metal makes these nanoshells biocompatible and because of this property they are lucrative for biomedical applications [16, 17].

2.1.1 Why Gold nanoshells?

In many cancers, tumor margins which are well characterized from normal tissues are treated or removed using conventional surgical technique. However, surgical removal is not possible in some cases which demands for alternate treatment technique. Also, in many cases conventional techniques may cause side effects, risks of complications and longer recovery periods hence greatly affects patient's life.

Therefore, I have employed this innovative nanotechnology in order to overcome these treatment complications and risks. Gold nanoshells are a new class of nanoparticles that consists of a dielectric core and coated by a thin layer of gold. These nanoshells are sensitive to particular wavelength of light and cause heating effect sufficient to destroy cancerous cells. This property of gold nanoshells led us to employ gold nanoshells to cause thermal ablation of tumor [18].

2.2 Optical properties of Gold nanoshells

Gold nanoshells are the new types of gold particles consist of a dielectric core (silica) covered with a thin layer of gold (shell). These nanoshells offer strong optical absorption of light due to the presence of metal layer, which is known as a shell. The reason behind coating of core with metallic layer comes from the fact that metallic coating permits strong interaction with electromagnetic waves. Upon exposure to electromagnetic waves, like light, these gold nanoshells demonstrate a strong interaction phenomenon known as surface plasmon resonance. As a result of surface plasmon resonance, there are oscillations in surface electrons of the nanoshells caused due to excitation by the energy absorbed from light. Using this phenomenon, nanoshells can be designed for particular application with the intention that their surface plasmon will resonate at a certain frequency of light. This phenomenon is an aid in the treatment of cancer as oscillations of surface plasmon efficiently converts light energy into heat [16, 20].

In response to light, the optical absorption mainly depends on the relative size of the nanoshells core and the thickness of the shell. Therefore, by altering the relative core

and shell thickness the optical response can be varied across a wide range of the optical spectrum which includes both the visible and NIR band. In addition, other factor like large cross-section, spectral tunability, absorption/scattering tunability ratio, electromagnetic near-field enhancement permit gold nanoshells to offer useful role as a thermal treatment agent [20]. In cancer treatment applications, treatment through light absorption property of gold nanoshells requires higher absorption cross-section with lesser scattering. In several cancer cases, tumor margins which are well characterized from normal tissues can be treated or removed using conventional surgical technique. However, conventional techniques may cause side effects, risks of complications and longer recovery periods hence greatly affect patient's life. Hence, surgical removal is not possible in every case which demands for alternate technique for treatment. Also,

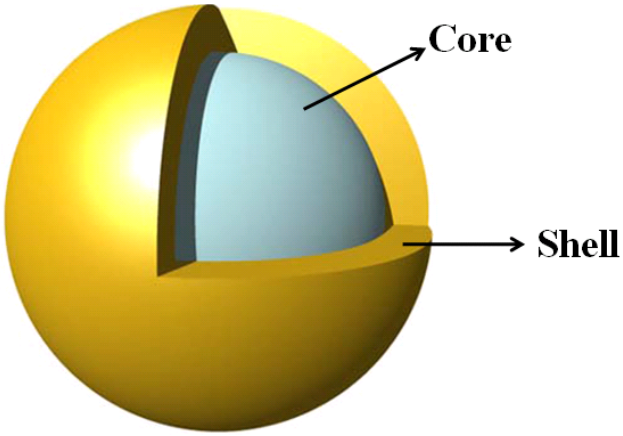

Figure 2.1 Structure of gold nanoshell [16].

2.3 Applications of Gold nanoshell in biomedical field

In the field of nanotechnology for complicated biomedical problems, gold nanoshells provide safe and unique solutions. Apart from their nanostructure, these nanoshells incorporate many features which are potentially ideal and exceptional for a single particle. The features of gold nanoshells that offer variety of application in biomedical field are biocompatibility, chemical functionality, and optical tunability in the near infrared. The two main applications which are possible are diagnostic and therapeutic biomedical applications. In diagnostic solutions, a significant function of nanoshells is to act as near infrared resonant that renders them to be optically detectable in whole blood. While in therapeutic solutions, these highly near infrared absorbing nanoshells can be employed as a heating tool to kill cancerous part. Near infrared light is employed for the excitation of nanoshells in order to aid photothermal destruction of cancerous growths in vitro as well as in vivo. Moreover, nanoshells can be specifically accumulated to certain tumor sites because of their nanostructure. The reason behind using gold for outer shell is that as an inert metal it offers various advantages over other nanoparticles. It provides numerous advantages which include biocompatibility, noncytotoxicity, and also it helps in conjugation to monoclonal antibodies and to other biomolecules for both active tumor targeting and biosensing applications. However, tunability may be the most novel and versatile feature of gold nanoshells [20].

2.3.1 Diagnostic applications of gold nanoshells

Cancer diagnosis is one of the most imperative and challenging area in the biomedical research. There are numerous techniques available for cancer imaging and out of which some have great potential in diagnosis. However, out of these techniques some suffer inaccuracy and cause complications, risks and side effects. With the emergence of nanotechnology, it is possible to diagnose different cancers with greater accuracy and less risks or side effects. Application of nanoshells as an imaging tool for cancer provides variety of advantages over other methods. But, the optical properties of gold nanoshells make them superior for imaging and upon accumulation these properties becomes further sensitive. As nanoshells accumulate, the absorption and the absorption spectra shifts at the original peak are reduced. As a result the scattering properties of nanoshells make them valuable for imaging purpose [21].

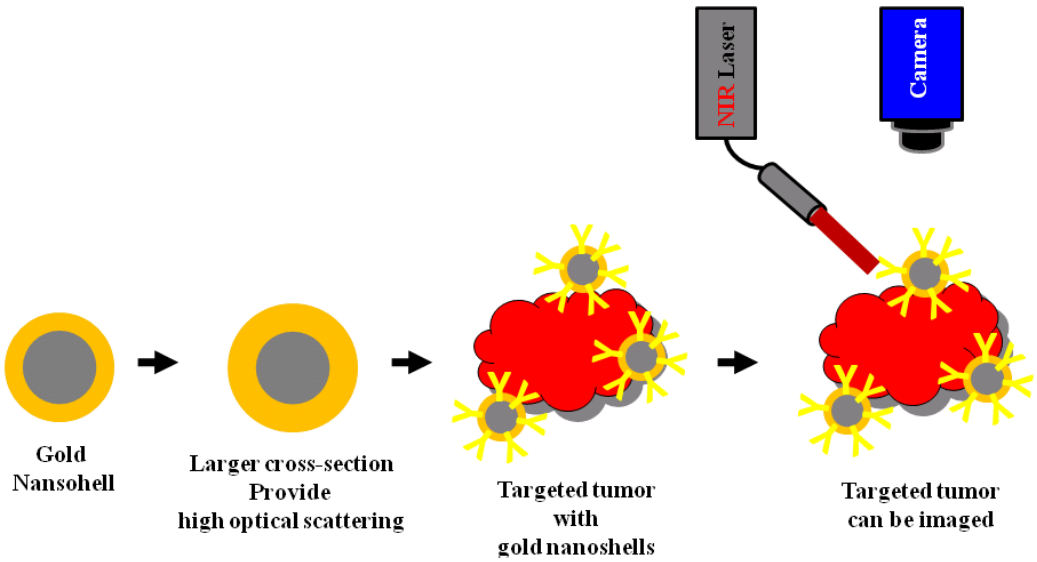

Figure 2.2 Application of Gold nanoshells in imaging cancer [23]

In cancer imaging, near infrared light are used to illuminate cancer targeted nanoshells which scatters back some amount of light from the tissue (figure 2.2). There are a number of techniques available to detect and capture back scattered light using camera and photo detectors. For results, amount of detected backscattered light helps to construct an image for further analysis.

2.3.2 Therapeutic applications of gold nanoshells

In this modern era, the remarkable growth in the field of nanotechnology has offered a range of nanostructures with unique properties which are valuable to biology and biomedical applications [23]. However, among all the applications the most fascinating and promising is the treatment of various cancers using thermal therapy. Furthermore, various destruction techniques for solid tumors using hyperthermia have been under research and in the past studies for thermal therapies numerous heat sources have been employed which include laser light, focused ultrasound, and microwaves. Thermal therapeutics is advantageous over conventional because of numerous reasons which include that they are minimally or non-invasive, relatively easy to perform, and tumors embedded within or located near vital tissue regions can be treated with more accuracy and ease where surgical resection may not be possible. In some situation, it is possible to perform surgical resection of solid tumors, which involves removal of well-defined, accessible, and for tumors not embedded within or located near vital tissue regions. But, due to the risks of high morbidity, invasive nature associated with surgical resection of small tumors embedded within or located near vital tissues, makes this therapy inappropriate for treatment. As an alternative to conventional treatment

therapies and surgical treatment for solid tumors, thermal ablation therapies can offer a minimally invasive way of destroying tumors by the application of heat.

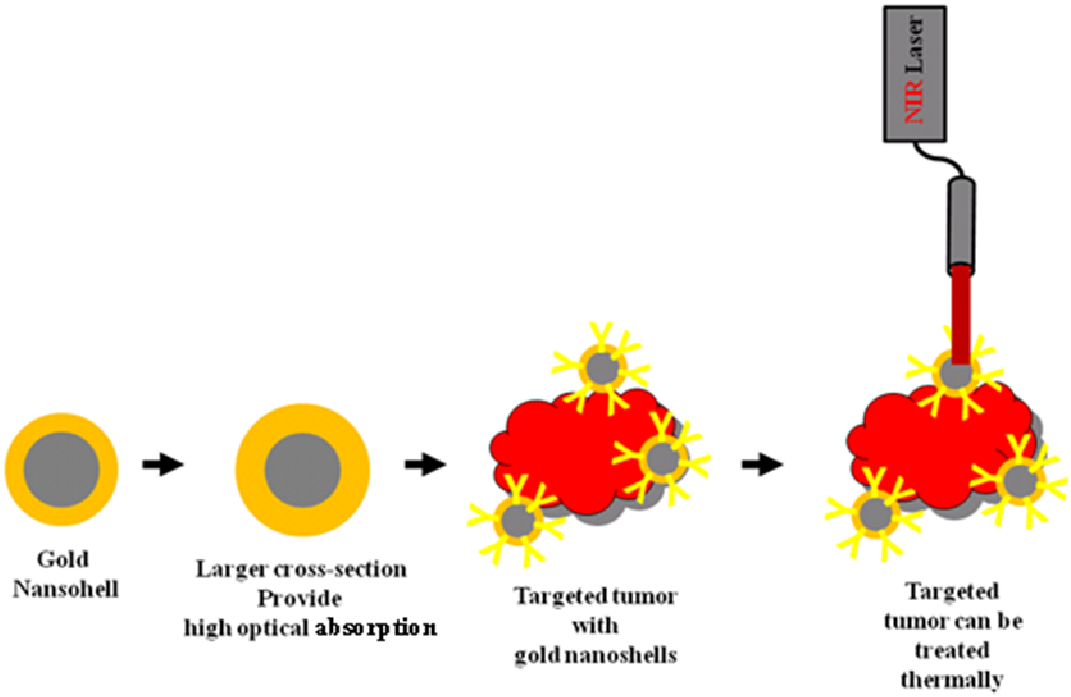

Figure 2.3 Application of Gold nanoshells in cancer treatment [24]

Also, these therapies are performed with ease and offer better recovery time with low risks. On the other hand, heat energy source to treat or destroy underlying tumors are required to adequately penetrate healthy tissues without harming them. However, conventional heating techniques are not completely successful and render difficulty in discriminating tumors from surrounding healthy tissues. Conventional heating techniques often heat intervening tissue between the heating source and the tumor, hence adding risk to patient's life [12]. In human body, the chromophores that amount for major absorption of light are water, oxygenated & deoxygenated hemoglobin. However, human body only permits certain wavelengths of light to travel

through the body and these wavelengths fall outside the visible spectrum [24, 25]. In electromagnetic spectrum, near infrared region offer tissue window, that permits optimal penetration of light through biological tissues. Therefore, deep penetrating NIR light is useful for treatment of tumor via hyperthermia. Hyperthermia is described as heating tissue by elevating temperature in the range of 41-47°C for some minutes, while the spread of heat is based on wavelength of light, tissue composition and blood perfusion [26].

Effective hyperthermia is difficult to achieve by solely laser application and many contrast agents (such as indocyanine green) have been used to overcome this drawback. However, successes with current agents and systems are not promising to effectively treat cancer. Therefore, I have implemented a new technique, interstitial laser induced hyperthermia (ILIH), mediated by a new class of NIR absorbing nanoparticles known as gold nanoshells [22].

CHAPTER 3

METHODS AND MATERIALS

3.1 Instrumentation

I have employed an integrated Fiber Array Pack, FAP-I system (Coherent, Santa Clara, CA, USA), which is a turn-key, fiber-delivered laser diode bar system as shown in figure 3.1, and is capable for many applications including medical therapeutics.

3.1.1 Laser diode FAP system

This Laser diode system is composed of a single enclosure which includes an integrated fiber array packaged (FAP-I) laser diode bar mounted on an air-cooled heat sink with all necessary drive and control electronics. This FAP-I includes integrated thermoelectric coolers in a sealed package, with control over laser diode temperature, as well as current and pulsed or continuous wave (CW) diode operation. The FAP-System is capable of delivering up to 30W of optical radiation/diode light into an armored 800µm core fiber. Optical radiation is delivered via a front panel mounted SMA 905 connector, which connects factory supplied armored 800 micron diameter transport fiber. The transport fiber is 5 meters long and sheathed in a stainless steel jacket which makes it easy to use and handle for new applications. These advantages make FAP-system flexible and an easy to use interface [27].

The FAP-system is rack mountable, plugs into a standard wall socket, and requires no water cooling, while it can be controlled either by the front panel user interface or by a computer-controlled RS-232 interface. This system offers a user-replaceable FAP-I diode module, which can also be replaced with different wavelengths allowing complete flexibility for the user. Also, it has imaging and collimating modules which offer different spot sizes and focal distances for various medical or pumping applications. However, a proprietary aiming module can be integrated with any of the imaging modules, to show the path and focus of the laser beam.

Figure 3.1 Laser diode FAP system and Optical transport fiber [27].

3.1.2 FAP

The heart of the FAP-system is the fiber array package (FAP-B) which consists of a laser diode bar with collection and symmetrizing optics mounted with an environmentally sealed package. The FAP-B efficiently converts the current supplied by the FAP-system electronics into a circularly – symmetric, multi-mode laser beam. The FAP-B is designed to operate under continuous wave (CW) or pulsed operating

conditions at high, multi-watt output power for thousands of hours. However, for our application the system was operated in continuous wave (CW) mode. At low drive currents, the laser diode bar will have insufficient gain to lase. In this system, some light, originating from spontaneous emission, will be visible emerging from the distal end of the optical transport fiber. As the drive current increases the laser diode bar reach threshold, where it will have sufficient gain to lase. This drive current is called threshold current. Furthermore, increase in current will cause a linear increase in output optical power up to the specified operating power [27].

3.1.3 Optical transport fiber

The FAP-I output laser beam is fiber delivered with a multi-mode, single core optical transport. Within the FAP-system enclosure is a short jumper fiber which transports the laser radiation from the FAP-I output to the front panel. At the front panel, the output from this short jumper is butted against the armored optical transport fiber as shown in figure 3.1. The transport fiber has an 800µm diameter fused silica core with a glass cladding. All optical interfaces are anti-reflection coated to minimize loss and optical feedback to the laser diode [27].

3.1.3.1 Beam laser fiber

A 600 micron bare fiber (Laser peripherals LLC) with a polished flat tip was used along with previously described optical transport fiber. This fiber transmits the laser energy in a forward direction and was coupled with armored optical transport fiber using a small connector as shown in figure (3.2). The fiber is 3.5 meters long and is terminated with an SMA-905 connector.

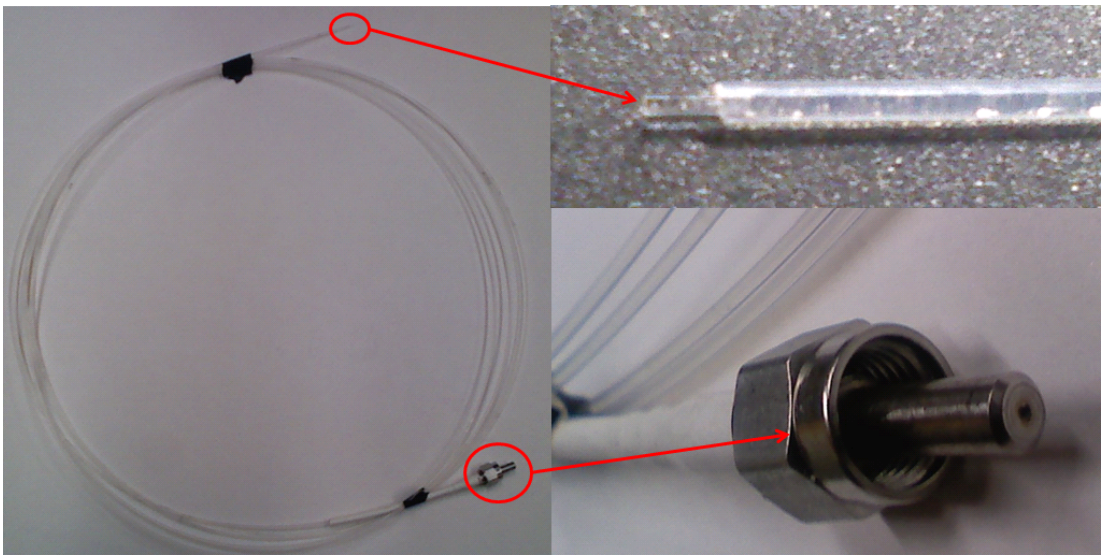

Figure 3.2 Beam laser fiber.

3.1.4 Power meter

The laser power meter model used for power measurement was FieldMaxII-TO (Coherent, Santa Clara, CA, USA). This power meter functions with a broad range of thermopile and optical sensors, but in this study I have used thermopile sensor for measurement as shown in figure 3.3. Together, this sensor enables FieldMaxII-TO to measure NIR laser output from the nanowatt to the kilowatt range, and to work with CW and pulsed lasers.

Figure 3.3 FieldMaxII-TO laser power meter and thermopile sensor.

3.1.5 Thermometer and thermocouple needle

A handheld thermometer (Omega Technologies, Stamford, Connecticut) along with a thermocouple needle were used to measure temperature (figure 3.4). The thermometer used accepts different types of thermocouple which include K, J, E, T, S type thermocouple. However, we have used T type thermocouple because of its sensitivity and wide range for temperature measurement. A hypodermic probe was used which comes with a type T (Copper-Constantan) element, 1.2 m (4') PFA-insulated lead wires, and uses a standard (21 gage) hypodermic needle 38 mm (1.5") long. 1.2 m (4') lead wire is a standard. Standard size male connector terminates the lead wire.

Figure 3.4 Thermometer and hypodermic thermocouple needle.

3.1.6 Data logger

The Hydra Series II (figure 3.5) is a 21-channel data logging instrument that measures and records temperature via thermocouples (T-type) at multiple measurement locations. Also, thermocouple reference junction compensation is automatically performed by sensing the temperature of the input module's isothermal block. An RS-232 serial interface makes it easy to connect the Hydra Data Acquisition Unit to a PC for real-time data acquisition. This Fluke hydra data logger also has removable memory data storage, internal memory storage, and direct real-time data transfer options. Also, the removable Universal Input Module enables fast, convenient set-up and reconfiguration. This module also has the ability to quickly connect and disconnect a Hydra to these various sites while leaving all sensors wiring intact.

Figure 3.5 Hydra series II data logger [28]

3.1.7 Thermocouple wire

High quality type “T” thermocouple wire with Neoflon PFA insulation and improved wire accuracy was used for temperature measurement. The measuring end was soldered and the other end was connected to Universal input module for temperature measurements.

3.2 Experimental Setup for Phantom study

3.2.1 Tissue simulating phantom

I have developed tissue simulating phantoms for different Gold nanoshell based heat source geometries. The main materials which were used to prepare these phantoms are Gelatin powder (Sigma, St. Louis, Missouri, USA), intralipid (Baxter, Deerfield, Illinois, USA), and water. I have used intralipid 20% which is a sterile, non-pyrogenic fat emulsion prepared for intravenous administration as a source of calories and essential fatty acids. It is made up of 20% soybean oil, 1.2% egg yoke phospholipids, 2.25% glycerin and water for injection. In addition to this, sodium hydroxide is added to adjust the pH so that the final pH of the product is 8[35]. The individual concentrations of these two materials (Gelatin powder and intralipid) results in different optical properties and hardness. However, I have used the same amount of intralipid and gelatin concentration for the two types of phantom geometries. [29, 30]

3.2.2 Gold nanoshell based heat source geometries

In the modeling experiment, phantoms were designed and built to examine the temperature profile for different heat source geometries.

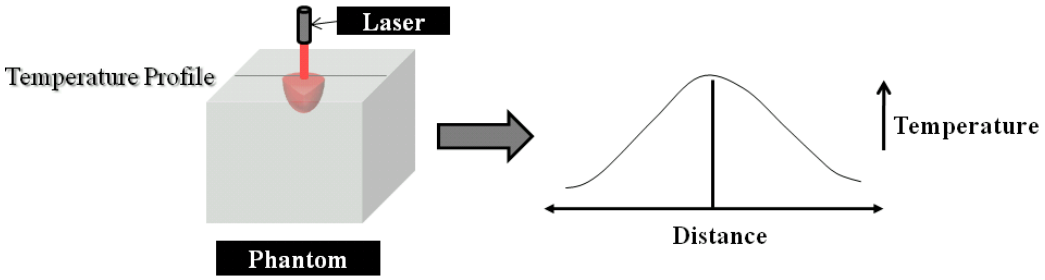

Figure 3.6 Schematic of temperature profile as a function of distance.

These phantoms were built to model and mimic gold nanoshells embedded tissue, by utilizing gold as a heat source in different phantom geometries. Along with the temperature profiles, this study also helped to determine the optimal relationship between the powers, concentration of gold nanoshell. These modeled gold nanoshell based heat source geometries are point heat source and single layered heat source.

3.2.2.1 Point heat source

This phantom geometry was aimed to mimic localized injection of gold nanoshells at the tumor site as shown in figure 3.7. Therefore, a simple tissue-simulating phantom geometry was built in a rectangular shaped plastic container of 10 cm x 5 cm x 5 cm (length x breadth x height). For gelatin-intralipid layer, 30 grams of gelatin powder (Sigma, St. Louis, Missouri, USA) made from porcine skin were added into 400 ml of boiling water and by stirring the warm solution was dissolved completely. Once the solution was cool down to 50 ° C, a solution of the 1% intralipid (IL) and 2.4 grams of paraformaldehyde was added to the prepared gelatin solution. Equal volumes (200ml) of the prepared gelatin solution and a solution of intralipid with paraformaldehyde were added, followed by stirring to dissolve it completely. This homogenous solution was then poured into the rectangular shaped plastic container and allowed for the formation of gel [29, 30].

Paraformaldehyde aids in increasing the melting temperature of the phantom by increasing the cross-linking of the fibers [32]. An array of conical shape cavities with a diameter of 3 mm was created using pipette tips on the top of the gelatin-intralipid phantom (figure 3.7). This was done before the formation of gel, by placing pipette tips

such that they were immersed ~4-5mm from the top surface of phantom to create cavities. The reason behind creating multiple cavities was to perform experiments multiple times for consistency. Before performing experiment, the developed empty cavities were then filled with 50µl of gold nanoshells solution.

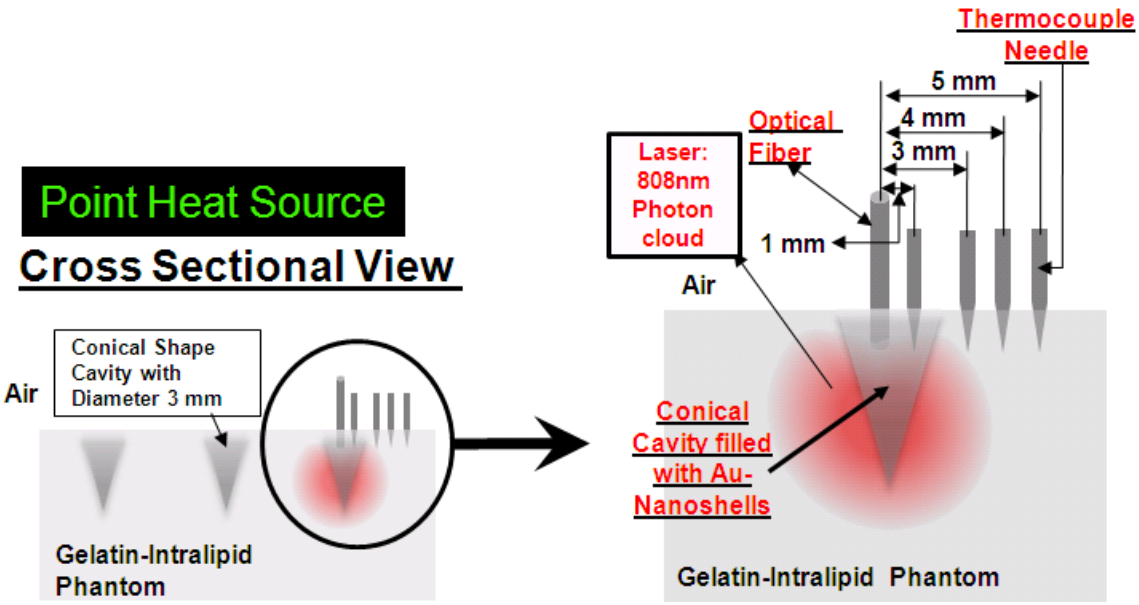

Figure 3.7 Cross sectional view of Gelatin-Intralipid phantom for point heat source geometry.

In point heat source experimental setup, the developed point heat source phantom geometry was used to perform experiments. As shown in figure 3.7, a conical shaped cavity is filled with a 50µl solution of gold nanoshells and an optical fiber (Laser peripherals LLC) is placed at a depth of ~1.5mm from the top surface. A hypodermic thermocouple needle is inserted at 1, 3, 4 and 5mm distance from the optical fiber in order to measure temperature. However, it is difficult to place or insert the needle at a distance of 2 mm i.e. at the periphery of the conical cavity. Therefore, temperature measurement was not performed at a distance of 2mm from the fiber or

from the site of illumination. As shown in figure 3.8, stand and holder are used to hold both the thermocouple needle and an optical fiber at a fixed position.

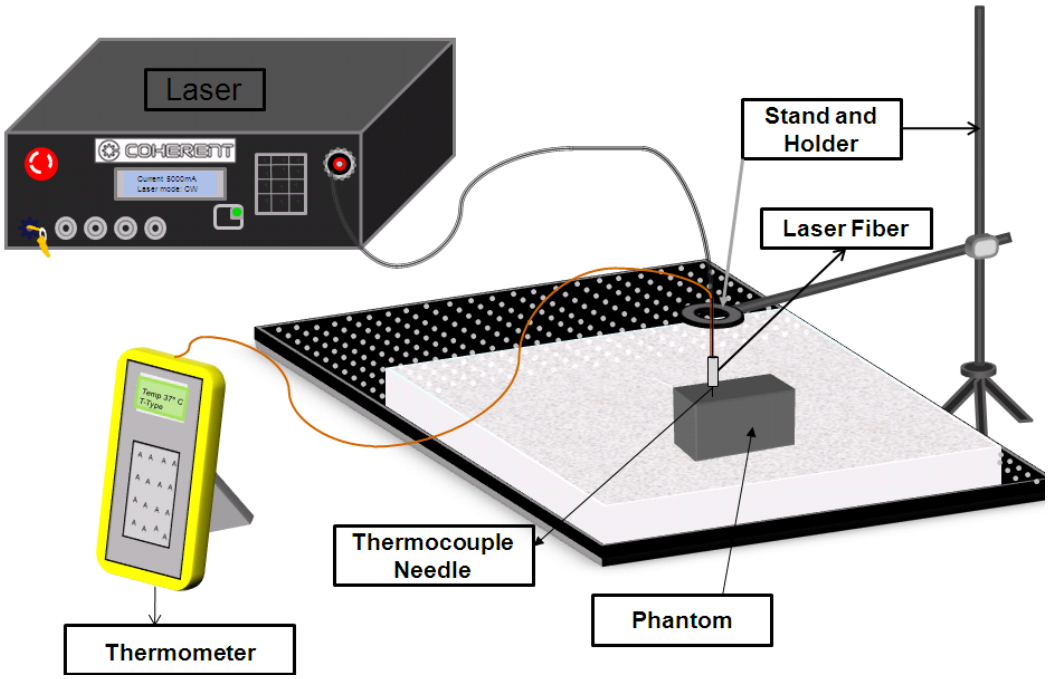

Figure 3.8 Schematic of setup for point heat source phantom geometry.

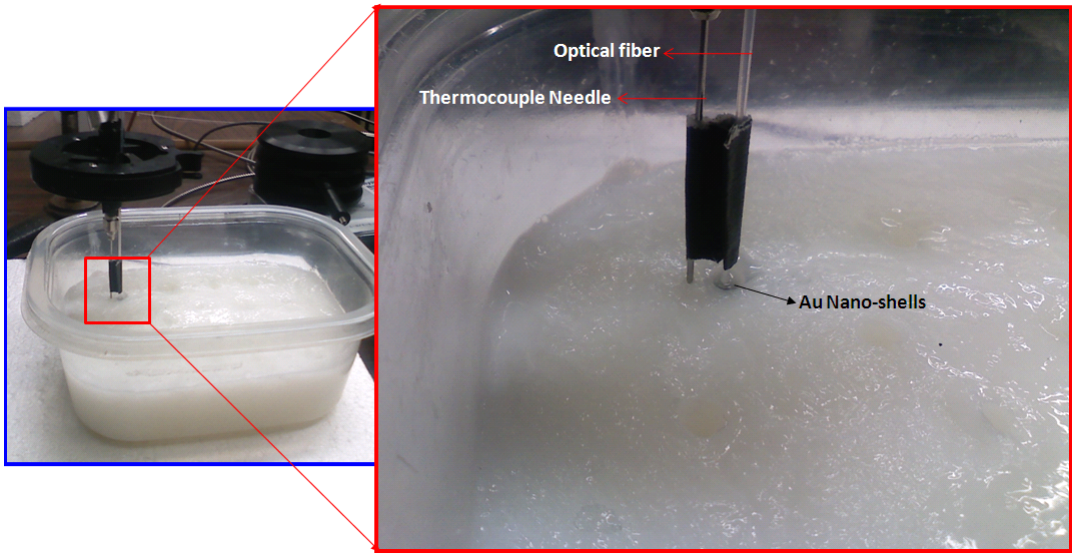

Figure 3.9 Actual setup in point heat source geometry.

One end of the optical fiber is inserted at a depth of ~1.5mm into the cavity while the other end is connected to the front panel of the FAP laser diode system (Coherent, Santa Clara, CA, USA) using a SMA connector. In figure 3.9, an actual setup is shown for point heat source geometry as described above.

Table 3.1 Experimental protocol employed on point heat source setup.

Exposure Time	Power	Power density	Concentration of Gold nanoshells in particles/ml			Distance
1 min	1W	7.96 W/cm^2	0.8e9	1.6e10	2.4e10	1,3,4,5mm
1 min	1.5W	11.94 W/cm^2	0.8e9	1.6e10	2.4e10	1,3,4,5mm
1 min	2W	15.92 W/cm^2	0.8e9	1.6e10	2.4e10	1,3,4,5mm

Table 3.1 summarizes the experimental protocol employed on point heat source geometry setup. The experiments were performed with 3 different power setting 1, 1.5, 2 W, while the calculated equivalent power densities are 7.96, 11.94, 15.92 W/cm^2 respectively. The conical cavities were filled with 50µl of gold nanoshells and the concentrations of gold nanoshells used were 0.8e9, 1.6e10, and 2.4e10 particles/ml. In addition, water was also used in one set of experiments to examine the difference in heating effect both from gold nanoshell and water. As shown in Table 3.1, the exposure time for all combination of experiments was 1min.

At the beginning of each simulation, finite numbers of photons are launched into the tissue with a predefined direction and position. Thereafter, photons of a defined light wavelength are propagated through the predefined tissue volume geometry that

has been assigned appropriate optical properties for each tissue type and photon wavelength.

3.2.2.2 Single layer heat source

A cubical plastic container of 5 cm x 5 cm x 5 cm (length x breadth x height) was used to built this tissue-simulating phantom geometry. Similarly for gelatin-intralipid layer, 30 grams of gelatin powder (Sigma, St. Louis, Missouri, USA) made from porcine skin were added into 400 ml of boiling water and by stirring the warm solution was dissolved completely. Once the solution was cool down to 50 ° C, a solution of the intralipid (IL) and paraformaldehyde was added to the prepared gelatin solution and was allowed for the formation of gel.

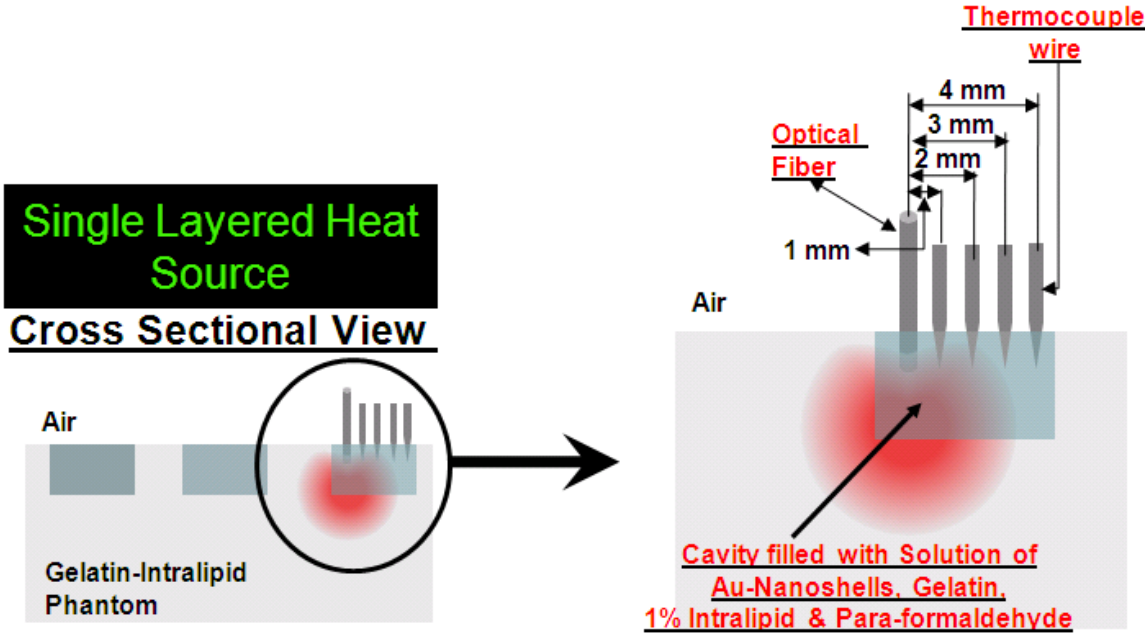

Figure 3.10 Cross sectional view of Gelatin-Intralipid phantom for single layer heat source geometry.

Paraformaldehyde aids in increasing the melting temperature of the phantom by increasing the cross-linking of the fibers. In this phantom geometry, an array of cubical shaped cavities with volume of 1000µl was created using cuvettes as shown in figure 3.11. Before the formation of gel, cuvettes were positioned such that they were immersed ~4-5mm from the top surface of phantom to create cavities. The reason behind creating multiple cavities is to perform experiments multiple times for consistency.

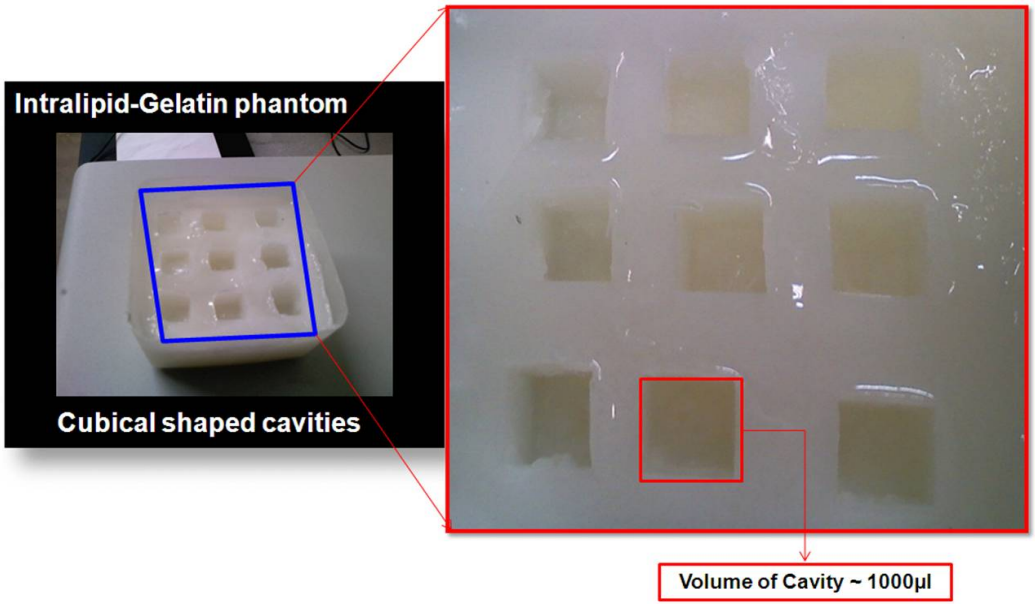

Figure 3.11 Top view of single layer heat source phantom after first step.

In the next step of phantom preparation, the empty cavities were then filled with a solution of 1% intralipid, gelatin, paraformaldehyde and gold nanoshell as shown in figure 3.12. The concentrations of gold nanoshells used were 0.8e9, 1.6e10, and 2.4e10 particles/ml.

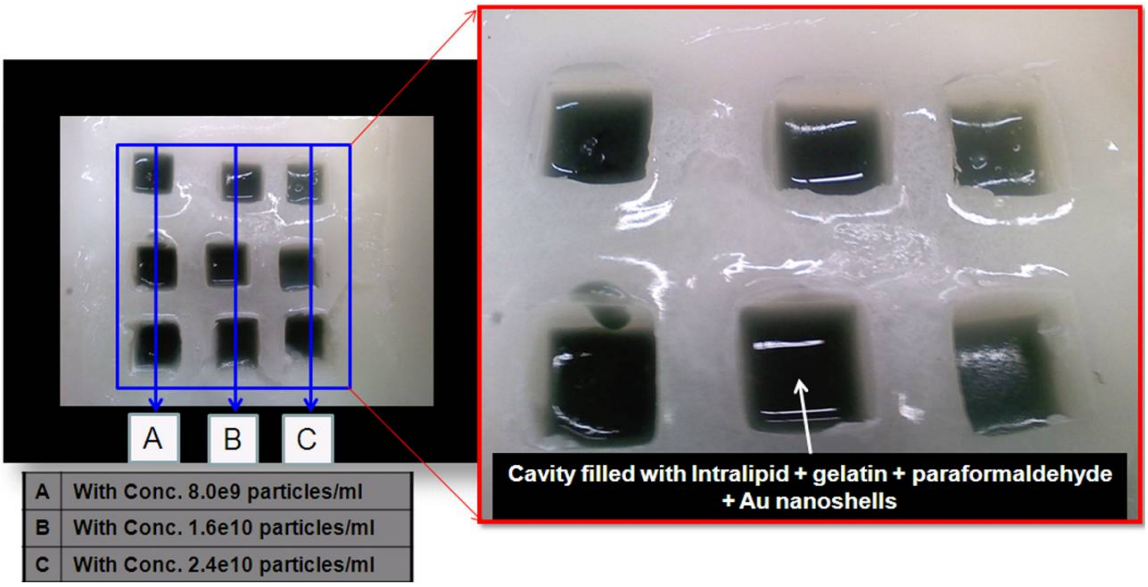

Figure 3.12 Top of single layer phantom after final step.

In single layer heat source experimental setup, the developed single layer heat source phantom geometry (figure 3.12) was used to perform experiments. As shown in figure 3.3 and figure 3.7, a cubical shaped cavity was filled with a solution of 1% intralipid, gelatin, paraformaldehyde and gold nanoshell and an optical fiber (Laser peripherals LLC) was inserted at a depth of ~1.5mm from the top surface. For this setup, hypodermic thermocouple needle was not used to measure temperature; as an alternative I have used T type thermocouple wires. Each of the T-type thermocouple wires were soldered at one end and the other ends were left as it is, in order to connect it with data logger. The positions of the four thermocouple wires were set at 1, 2, 3, and 4 mm away from an optical probe as shown in figure 3.13. This set position of the thermocouple wires and an optical fiber was then inserted at a depth of ~1.5mm (figure 3.15), while the other ends were connected to the hydra series II data logger.

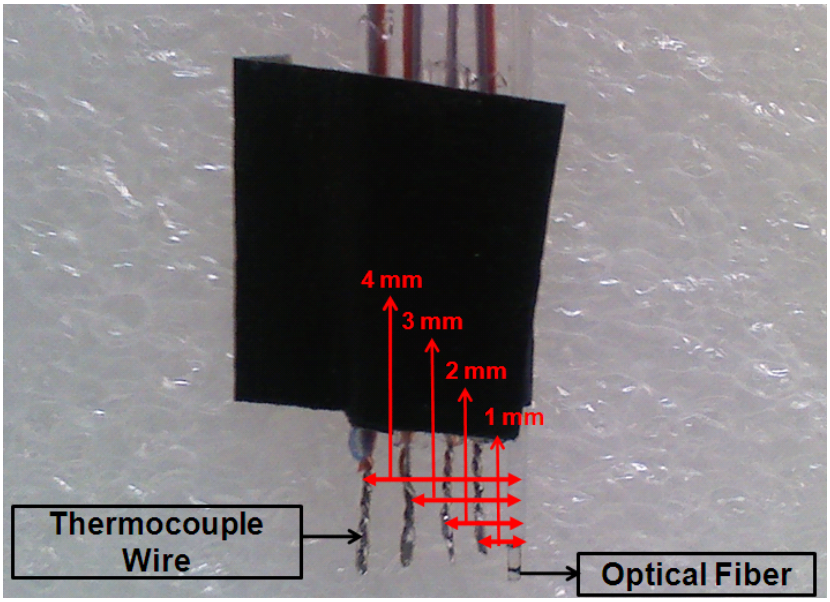

Figure 3.13 Thermocouple wires and optical fiber position.

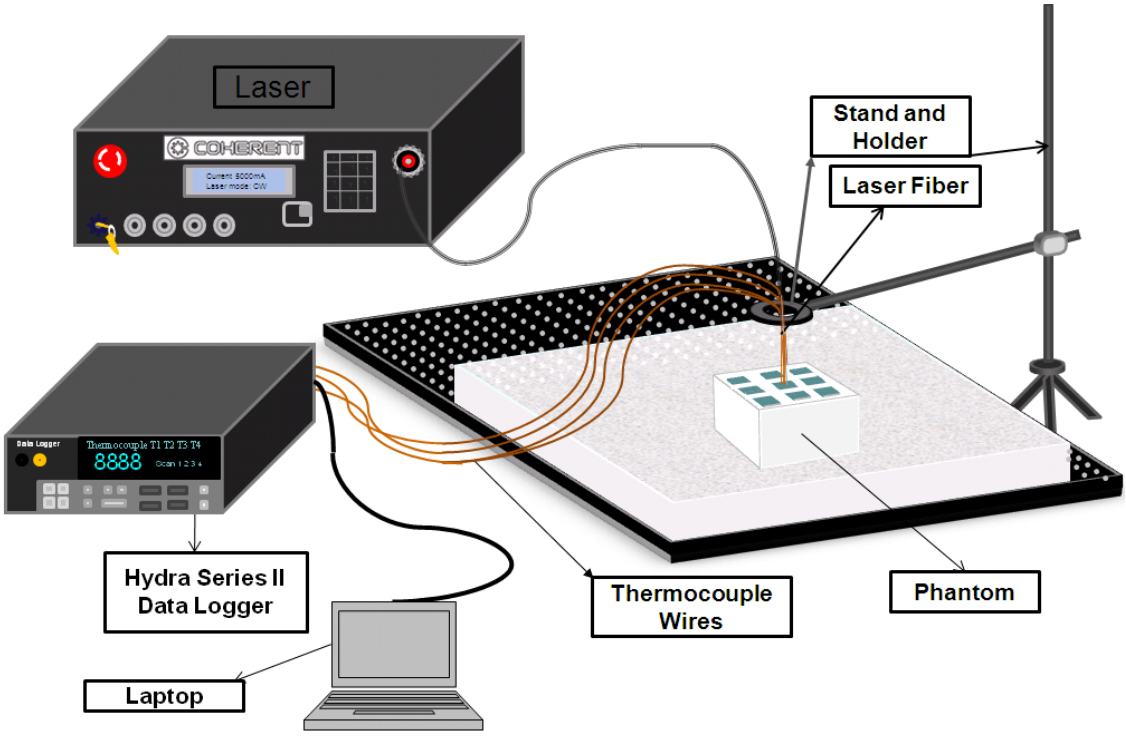

Figure 3.14 Schematic of setup for single layer heat source geometry.

Hydra series II data logger also offer RS-232 computer interfacing and therefore, temperature measurement and recording was performed using application software provided with the instrument. Stand and holder are used to hold both the thermocouple needle and an optical fiber at a fixed position as shown in figure 3.14.

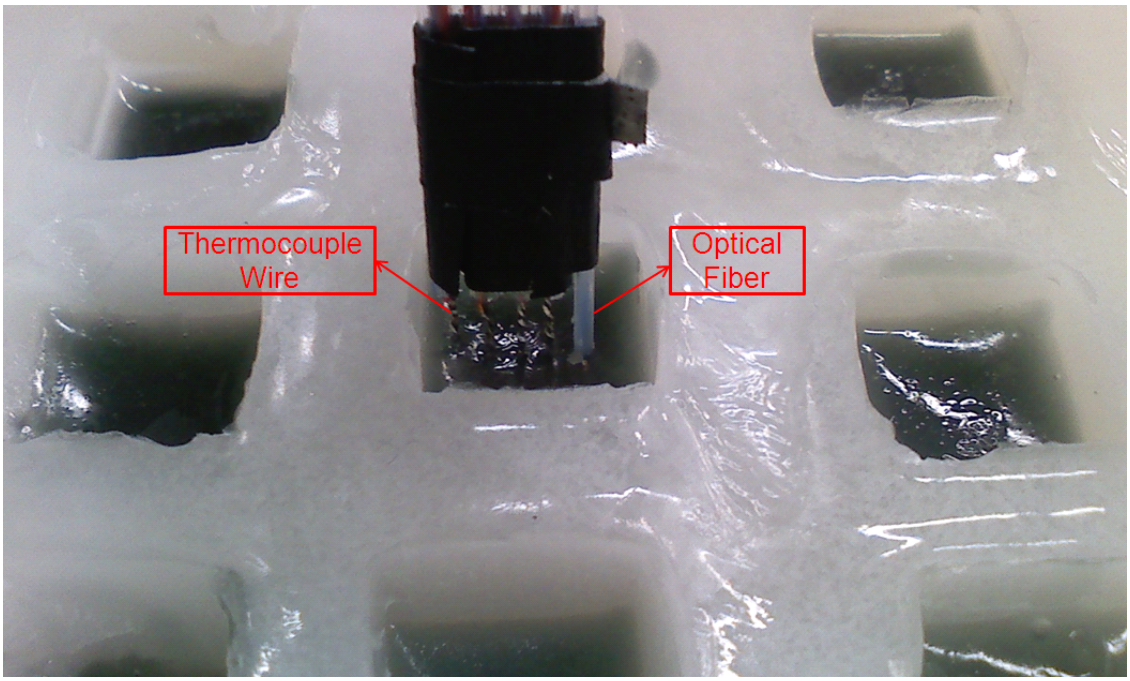

Figure 3.15 Actual setup in single heat source geometry.

The above figure 3.7 shows an actual setup in single layer heat source geometry. I have employed a similar experimental protocol as used in point heat source geometry, so as to compare the heating effect in the two different phantom geometries. However, it was easy to measure temperature at 2mm away from optical fiber in this setup, which was not possible in point source geometry setup.

3.3 Experimental Setup for Chicken tissue study

The reason for performing experiments on chicken tissue is to confirm phantom study results and to validate optimal experimental parameter setting for animal study. Therefore, I have used normal chicken breast tissue for our experiments. Similar kind of experimental setup was used as in phantom study, but with some changes. I have used an optical transport fiber laser delivery, not the beam laser fiber as used in phantom study. As shown in figure 3.16, holder and clip were used to hold the thermocouple wires and the laser fiber because of the limited area for fiber and thermocouples placement.

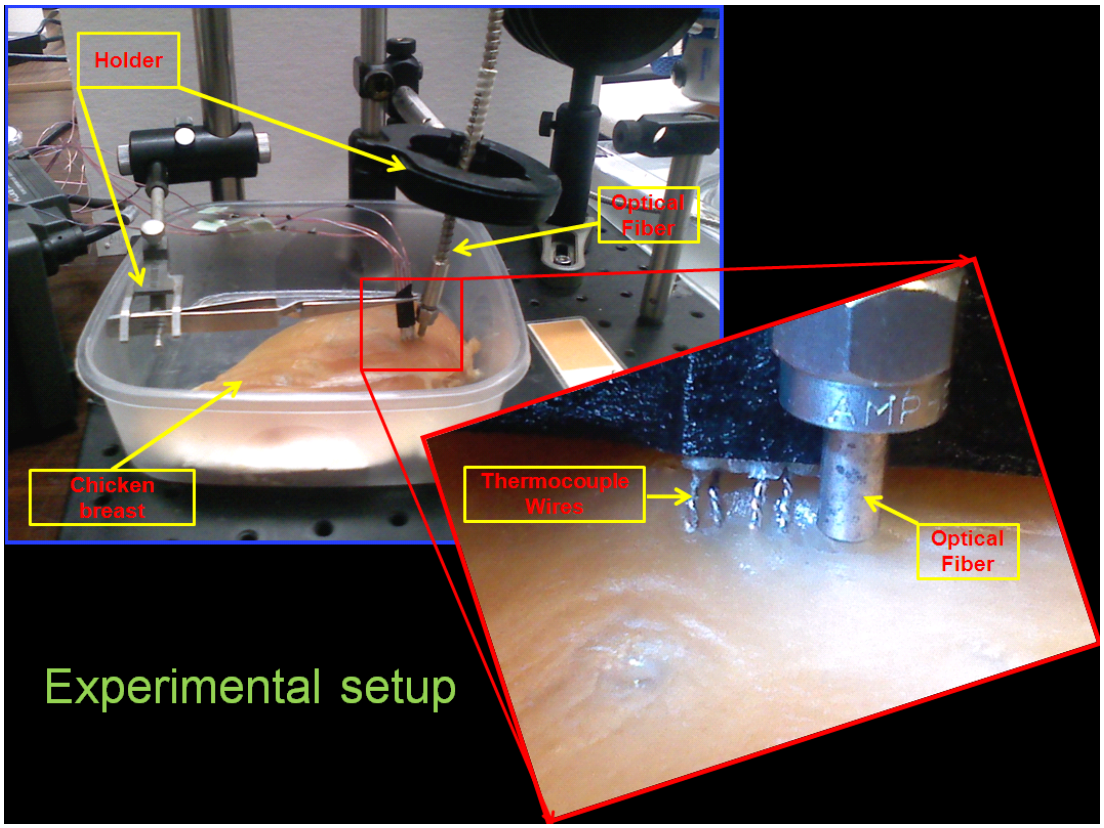

Figure 3.16 Chicken tissue study setup.

In this study, I have employed a modified protocol to see heating effect for longer exposure time. At multiple sites gold nanoshells dosages were injected, this was done by creating a small pocket using syringe and nanoshells were injected using micropipette. This is done so as to efficiently embed tissue areas with gold nanoshell and to avoid overflow of nanoshells. Here I aimed to determine optimal power setting for longer exposure time which was not performed in the phantom study.

3.4 Animal preparation and experimental setup

For preliminary study, I have also used two Copenhagen rats at age of 2 months and with weights ~300gms. The animal preparation and handling during the experiments were carried by Dr. Jinhui Shen, post doctoral research associate working with Dr. Liping Tang, Department of Bioengineering at UT Arlington. Rats were anesthetized for 4 minutes for hair removal from the back where the cancer cell line was injected. Prostate tumor cells (PC-3 cell lines) were injected bilaterally subcutaneously on the fore back of male rats under gas anesthesia. The tumors growth was monitored daily, and the tumor diameters were measured every other day to determine the volume. The tumors were allowed to grow until they reach a diameter of ~1cm as shown in figure 13.7.

Figure 3.17 Rat after developed prostate tumor bilaterally.

The rats with tumors of size ~1cm were anesthetized and maintained under general gaseous anesthesia with 1-3% isoflurane in air (1 dm^3/min). Tumors were shaved and a very small incision was placed to inject gold-nanoshells and to place optical fiber for treatment. Rats were placed on a temperature-controlled, warm blanket to maintain their body temperature. Prior to laser treatment, 50µl of gold nanoshells doses with concentration 2.73×10^{10} particles/ml were injected through syringe at different tumor location for treatment. After injections, an optical fiber coupled to the 800-µm laser was used to expose the laser light to the gold nanoshells-embedded tumor by placing the fiber interstitially at a site of injection with ~1mm depth. The integrated Fiber Array Pack, FAP-I system (Coherent, Santa Clara, CA, USA), as shown in figure 3.1, was employed to deliver 808 nm near infrared light at the tumor bed for 5 minutes.

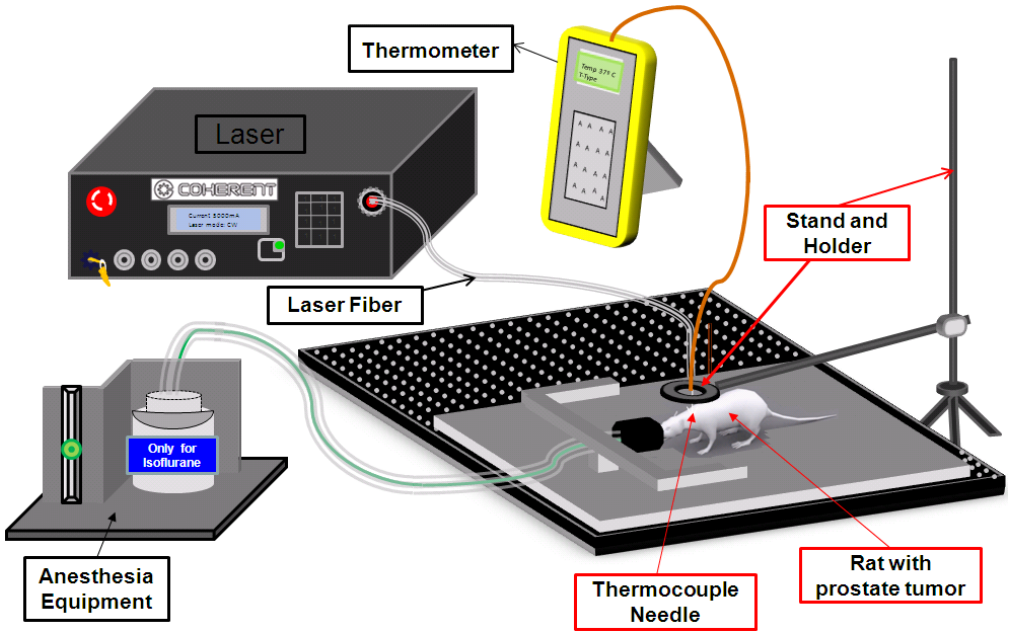

Figure 3.18 Schematic of setup for single layer heat source geometry.

Temperature in the vicinity of the treatment area was monitored during laser activation, using thermocouple needle (Omega Technologies, Stamford, Connecticut). This was done to avoid overheating of the treatment site which may cause tissue carbonization. The overall setup is shown in fig. 3.18. Care was taken to avoid any movement of laser fiber and thermocouple needle. During the experiments, the rats were injected at multiple locations with different gold nanoshells concentrations and consequently thermally treated.

CHAPTER 4

RESULTS AND DISCUSSION

4.1 Phantom study results

This study was aimed to investigate the optimal relationship between power and concentration of gold nanoshells, intended for effective heat spread over vicinity. Temperature profiles for different tissue phantom geometries, which simulate gold nanoshells embedded tumor from different injection schemes, were examined. As discussed in chapter 3, experiments were performed on different phantom geometries, with different combination of power settings and gold nanoshell concentration. I defined change in temperature ΔT (°C) as the difference in temperature attained after laser exposure and the temperature measured before laser exposure (base temperature). Following sections discuss the comparison of change in temperature ΔT (°C) as a function of time and distance for different gold nanoshells based heat source phantom geometries.

4.1.1 Point heat source geometry

In this section, a comparison between experiments performed using water and different gold nanoshell concentrations with different power settings are discussed.

Figure 4.1 shows ΔT (°C) as a function of power and distance for water and 3 different gold nanoshell concentrations. It can be observed from the 3D-plot that the there is an insignificant change in temperature ΔT (°C) with water for different power settings, a compare to different gold nanoshell concentrations. This may signifies that there was less absorption of NIR light by water as compare to gold nanoshells. Conversely, for same laser power setting and different gold nanoshell concentration considerable heating effect ΔT (°C) was observed, which could be due to high absorption of light by more gold nanoshells.

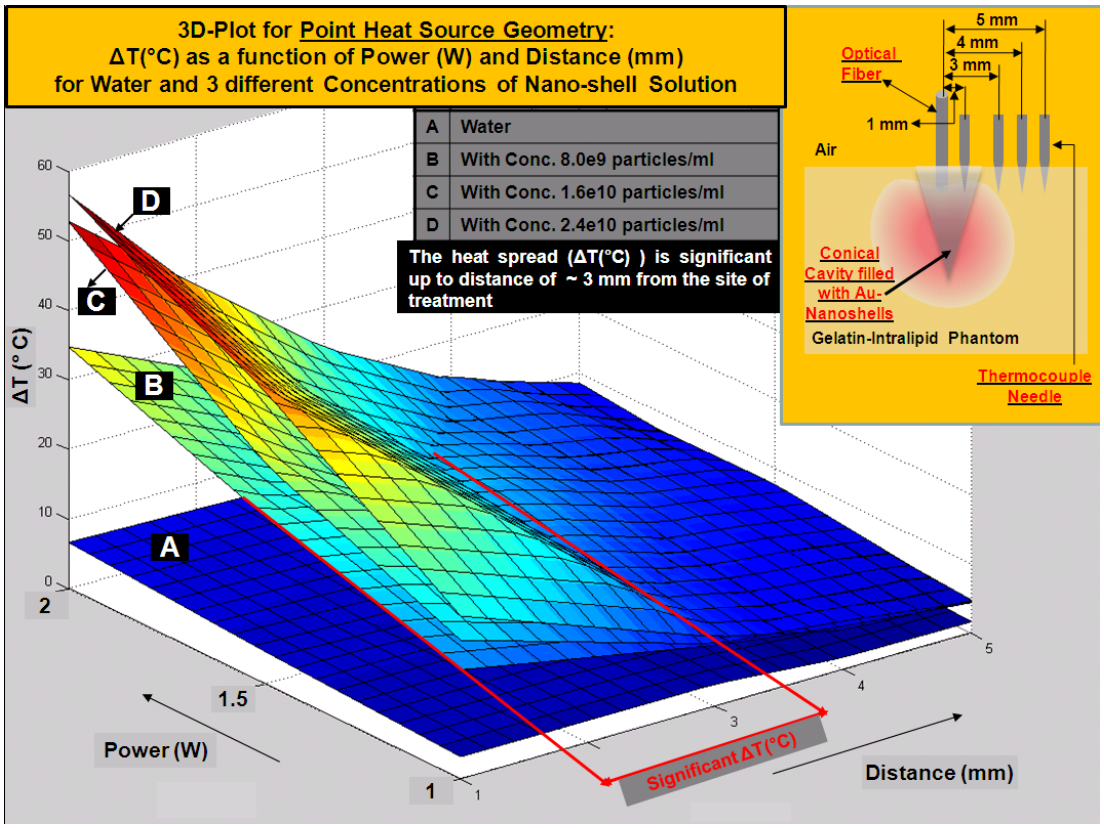

Figure 4.1 3D-plot comparing ΔT (°C) as a function of power and distance for water and different gold nanoshell conc. 0.8e10, 1.6e10 and 2.4e10 in point heat source geometry.

Although, significant change in temperature was observed using gold nanoshells but this change is limited to vicinity. Therefore, experiments with higher power setting and higher gold nanoshells concentration were carried out, with the aim of exploring heat spread from the site of laser illumination. Figure 4.1 shows that change in temperature ΔT (°C) decays fasters over vicinity even with higher power settings and higher gold nanoshells concentration. Thus, even higher ΔT (°C) observed for higher laser power and higher gold nanoshells concentration around the point of illumination but it is limited up to ~3mm.

4.1.2 Single layer heat source geometry

As discussed earlier, this model was aimed to simulate gold nanoshell embedded tissue. From the previous model, I estimated an optimal relationship between the parameter which can be useful for further study on phantoms and animals. In this section, a same experimental protocol was employed in order to characterize the two different phantom models.

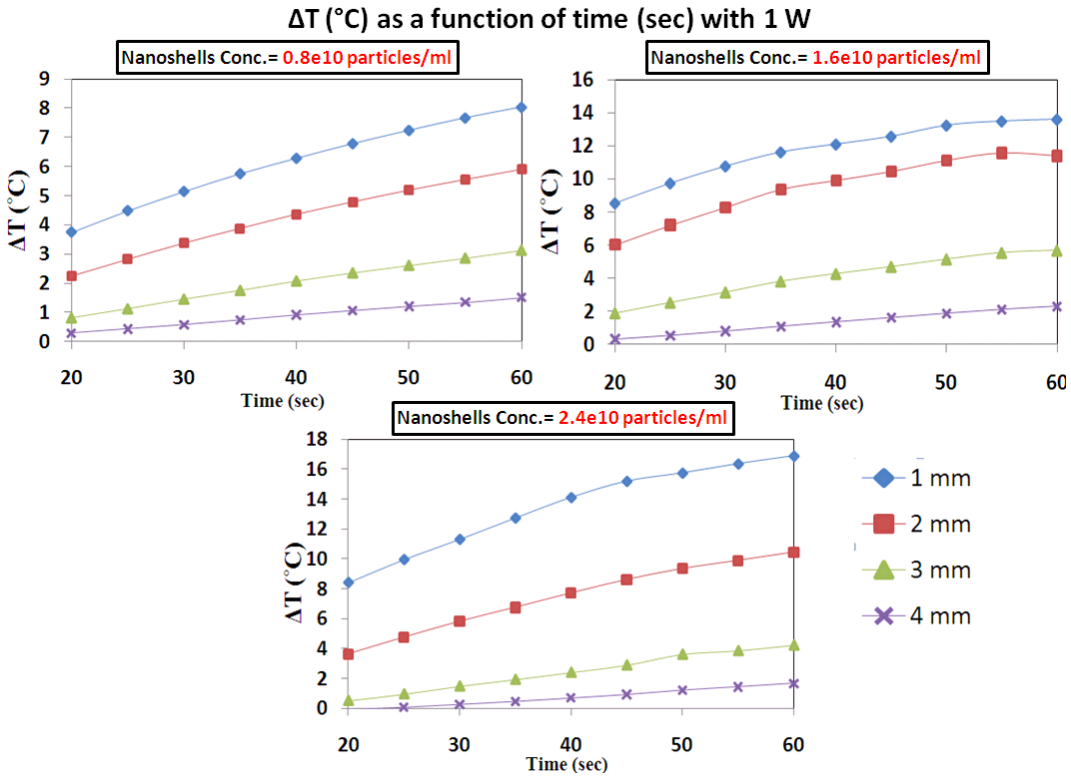

Figure 4.2 ΔT (°C) as a function of time for nanoshell conc. 0.8e10, 1.6e10 and 2.4e9 particles/ml and 1 W power in single layer heat source geometry.

Figure 4.2 shows change in temperature ΔT (°C) as a function of time (sec) for 3 different gold nanoshell concentrations when 1W power was employed for 1min. It can be observed that ΔT (°C) increases with the concentration of gold nanoshells, but ΔT (°C) decays faster as I move away from the point of illumination. As far as this model is concerned, the reason behind faster decay of ΔT (°C) may be due to localized absorption of light photons resulting in less number of photon absorption in the surrounding area. This explanation may justify the observed local heating effect.

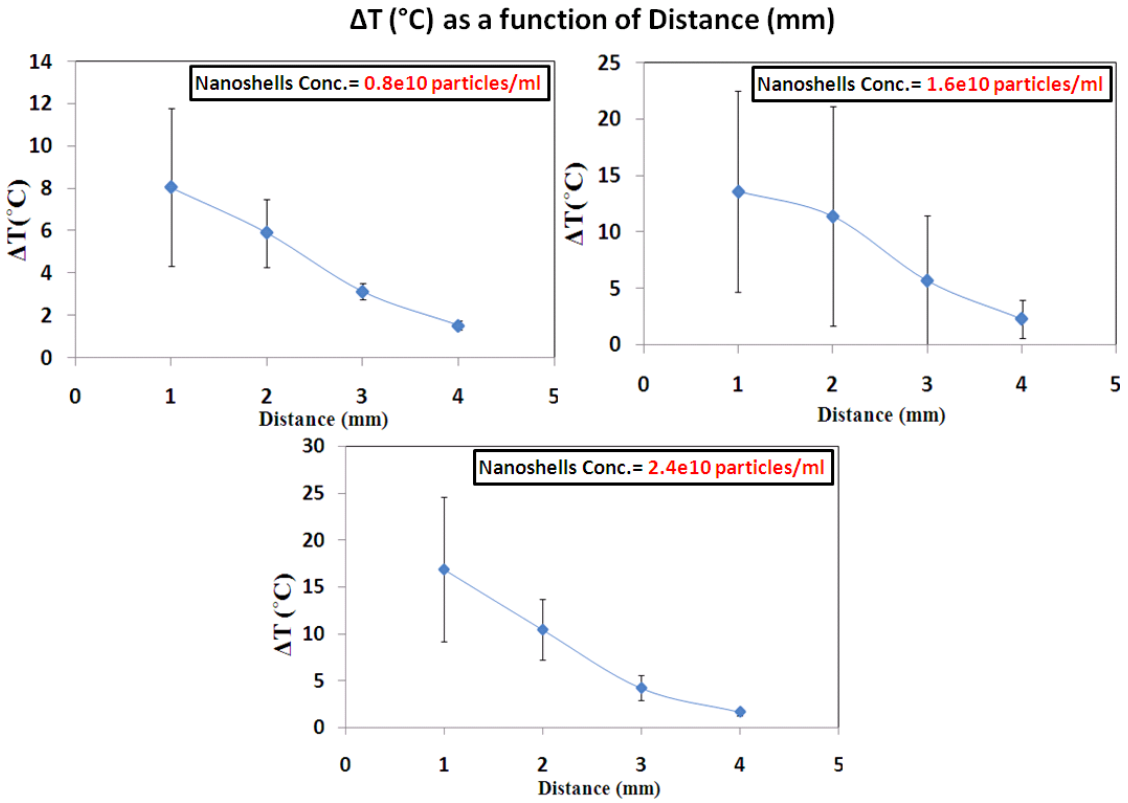

Figure 4.3 ΔT (°C) as a function of distance for 3 different gold nanoshell concentrations 0.8e10, 1.6e10 and 2.4e10 particles/ml and 1 W power setting in single layer phantom model.

Figure 4.3 above shows temperature profiles for 3 different concentrations of gold nanoshells with 1 W power setting and 1 min exposure time. This figure shows heating effect increases with the concentration of gold nanoshell, but not significantly over the surrounding area. It can be noticed in figure 4.3 that the change in temperature at 2mm for gold nanoshell concentration of 1.6e10 particles/ml was higher as compare to 2.4e10 particles/ml. The possible reason behind could be false temperature measurement and which may be caused by improper placement of thermocouple wires, or may be due to discontinuity in phantom surface. However, there are factors such as

optical properties of phantom, inadequate gold nanoshells may account in insignificant heat spread over surrounding area.

In the next step, to investigate the effect of higher powers on heat spread I attempt another set of experiment. Figures 4.4 and 4.5 show results with 1.5 W power setting. Figure 4.5 shows ΔT (°C) as a function of distance (mm) and I observe rise in the slope of curves which means that there was significant change in temperature within the radius of ~3mm.

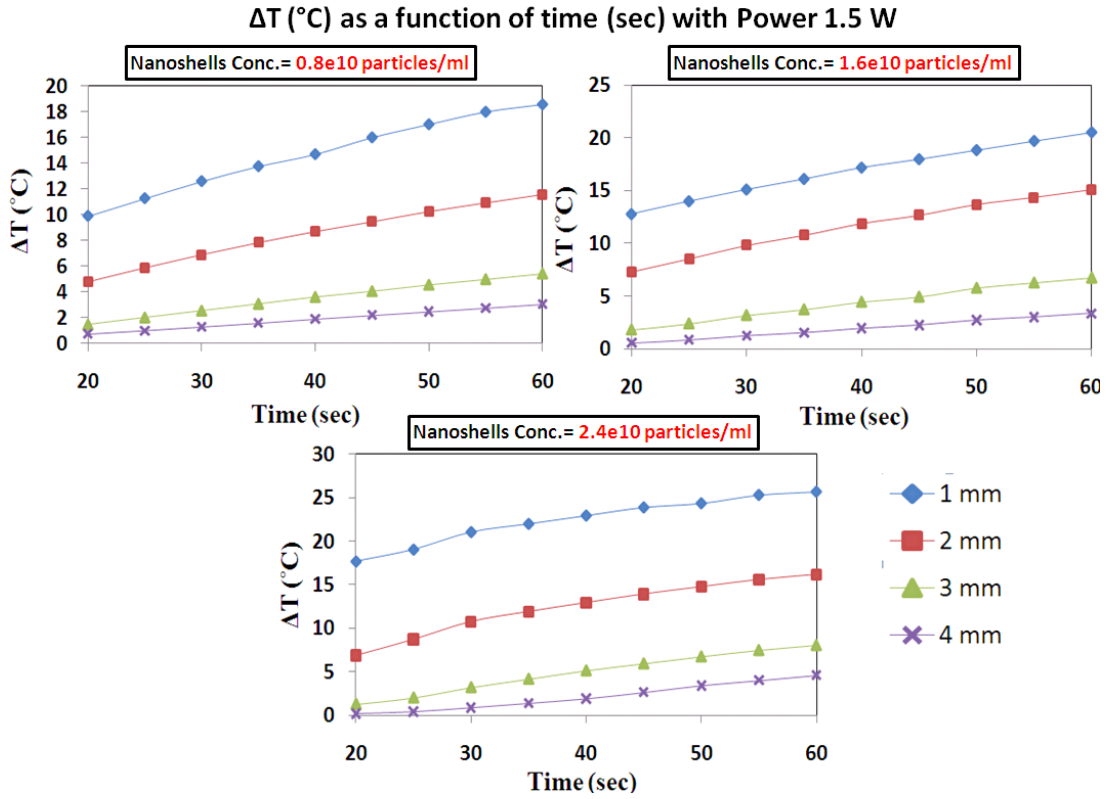

Figure 4.4 ΔT (°C) as a function of time (sec) for nanoshell conc. 0.8e10, 1.6e10 and 2.4e9 particles/ml and 1.5 W power in single layer heat source geometry.

Also, Figure 4.4 shows rise in ΔT (°C) for 1 min exposure of laser at 1, 2, 3, 4 mm. I deduce from the these results that though there is an increase in ΔT (°C) while

employing higher power, the significant change ~10°C is limited within the radius of 3mm circle.

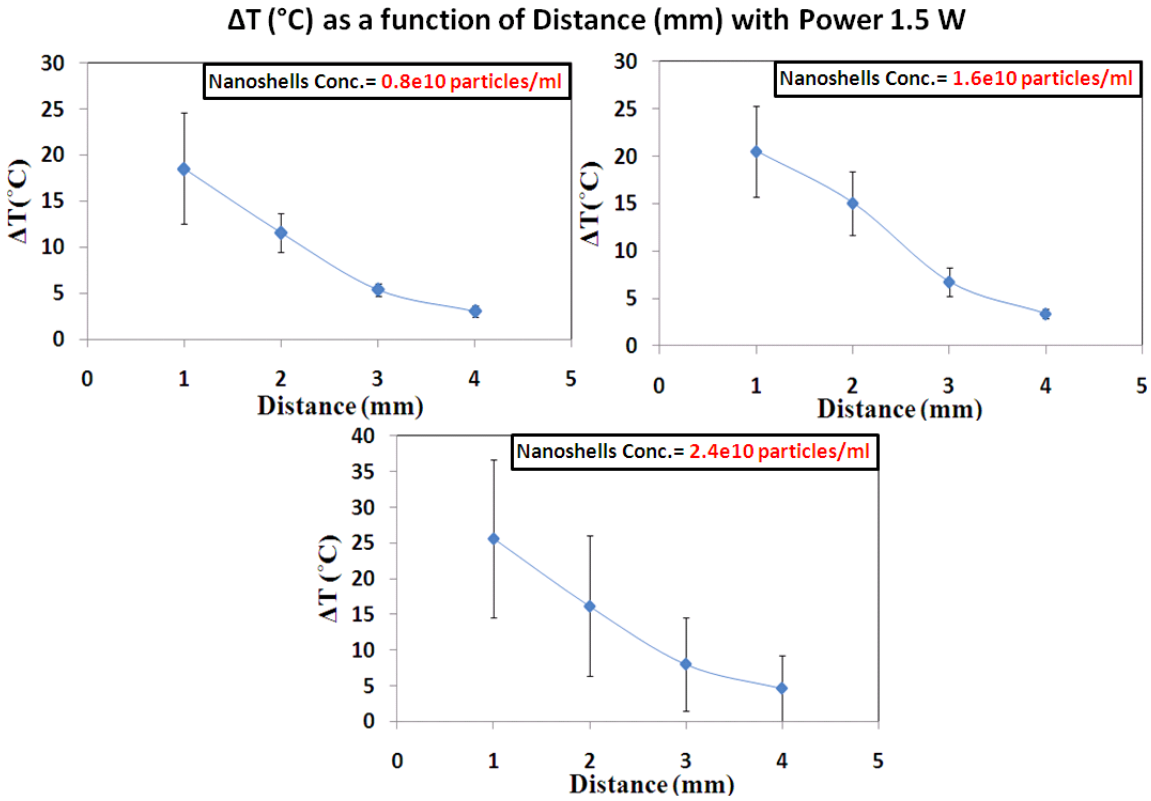

Figure 4.5 ΔT (°C) as a function of distance for 3 different gold nanoshell concentrations 0.8e10, 1.6e10 and 2.4e10 particles/ml and 1.5 W power setting in single layer phantom model.

Figure 4.6 and 4.7 shows ΔT (°C) for the highest power employed with the hope to see significant heat spread over larger area, which was not observed in previous settings. In this set, the different gold nanoshell concentrations used were same and the exposure time was kept 1 min. Again, rise in ΔT (°C) was observed with increase in concentration of gold nanoshells. However, it shows similar trend as was observed with lower power settings, i.e. the coverage area was within the radius of ~3mm. The 3 graphs in Figure 4.6 shows ΔT (°C) as a function of time (sec) for the 3 gold nanoshell concentrations 0.8e10, 1.6e10 and 2.4e10 particles/ml.

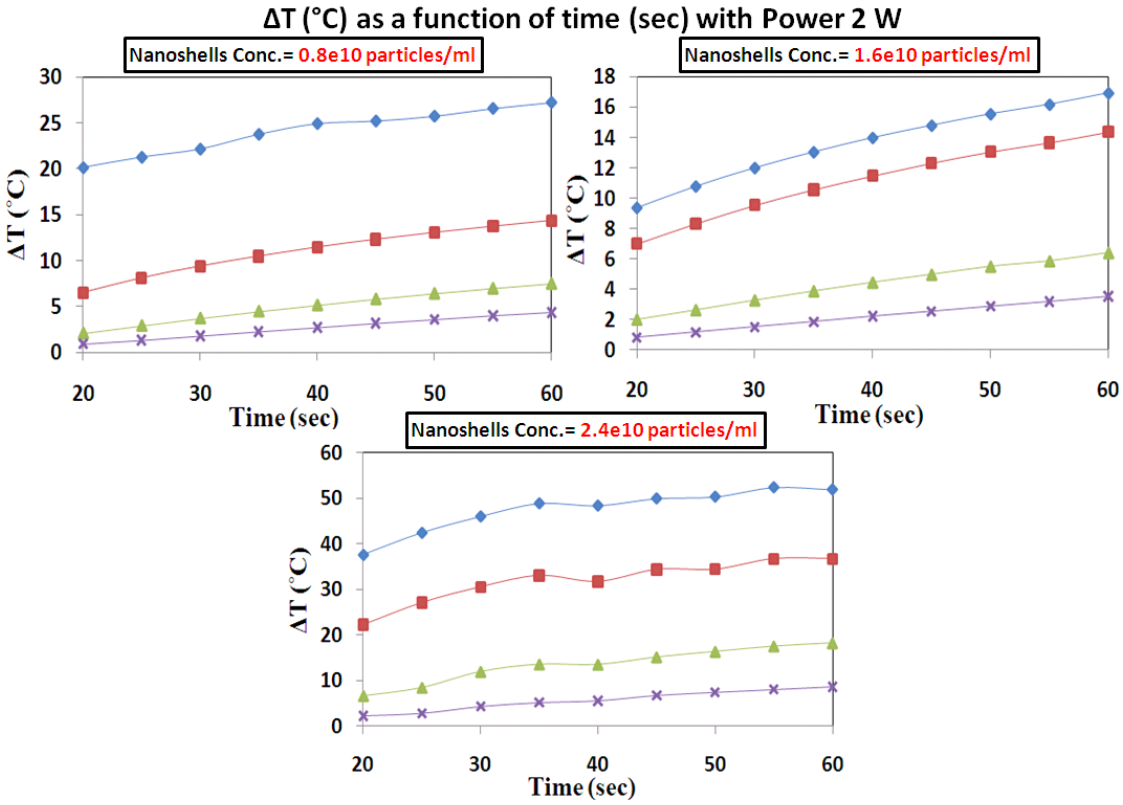

Figure 4.6 ΔT (°C) as a function of time (sec) for nanoshell conc. 0.8e10, 1.6e10 and 2.4e9 particles/ml and 2 W power in single layer heat source geometry.

This can be noticed from these graphs that there is some inconsistency in the result, as ΔT (°C) for gold nanoshell concentration 1.6e10 particles/ml shows lower values compare to the other two concentrations. The reason behind this inconsistency is may be due to discontinuity in phantom surface, improper placement of laser fiber and thermocouple wire.

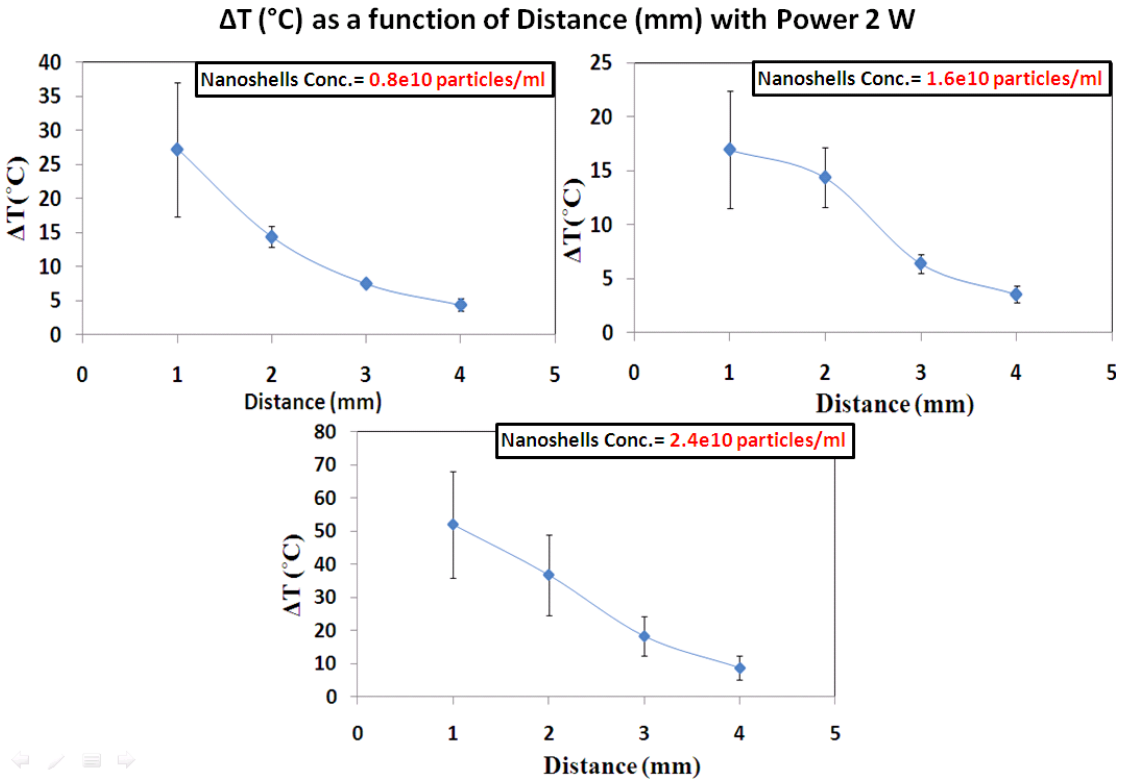

Figure 4.7 ΔT (°C) as a function of distance for 3 different gold nanoshell concentrations 0.8e10, 1.6e10 and 2.4e10 particles/ml and 2 W power setting in single layer phantom model.

It can be deduced that a higher laser power can assist heat spread in the presence of high gold nanoshells concentration. As in figure 4.7 ΔT (°C) for gold nanoshell concentration 2.4e10 particles/ml differ significantly as compared to other concentrations and power settings. In this case, ΔT (°C) is significant up to ~4mm with

highest change of 50°C was observed at 1mm. Despite the fact that higher laser power would be helpful for greater heat spread, it is desirable to employ lower power for biological tissue. This is to avoid over heating which may lead to carbonization of tissues.

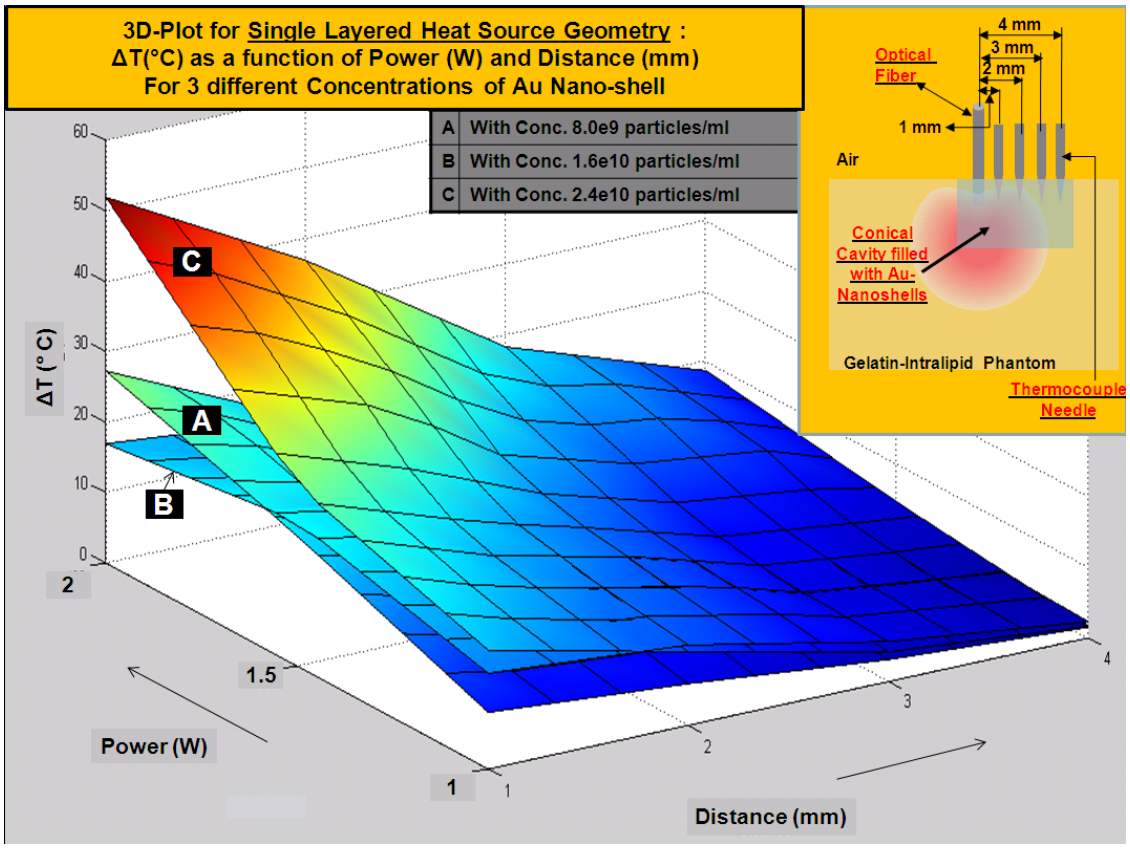

Figure 4.8 3D-plots comparing ΔT (°C) as a function of power and distance for different gold nanoshell concentration 0.8e10, 1.6e10 and 2.4e10in single heat source geometry.

Above figure 4.8 shows similar 3D-plots for single layer heat source phantom model as demonstrated for point heat source model. Basically, this 3D plots illustrate overall summary of the results for experiments performed on single layer phantom model with different protocol. On comparing with point heat source results, similar fashion have been observed for different power settings and gold nanoshell

concentrations. But, for single layer phantom model highest change in temperature achieved was lower (~10 °C) than the point source geometry. The reason behind inconsistency observed, as shown in figure 4.8 plot B with gold nanoshell concentration 1.6e10 particles/ml shows lower values as compare to 0.8e10 particles/ml in plot A, is discussed earlier in this section.

4.2 Chicken tissue study results

Apart from the phantom study, to examine the feasibility of the proposed technique on real biological tissues, chicken breast sample study was performed. The idea was to characterize optimal parameter settings for real tissue based on phantom study results. An attempt was made to repeat similar experiment performed on phantoms, at the same time some modifications were done in experimental protocol for further details. As discussed in chapter 3, measurements were performed with longer laser exposure times and also for different power settings.

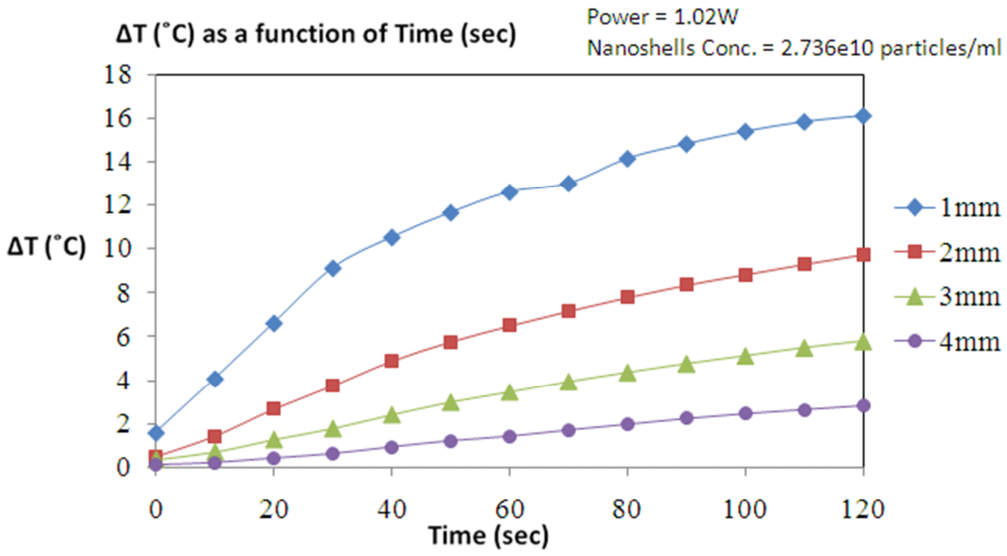

Figure 4.9 ΔT (°C) as a function of time for nanoshell conc. 2.73e10 particles/ml and 1.02W power in chicken breast sample.

Figure 4.9 shows the ΔT (°C) as a function of time for nanoshell conc. 2.73e10 particles/ml and 1.02 W laser power setting. Laser exposure time in this experiment was 2 minutes unlike exposure time used in phantom study. Temperature at every 10 seconds was measured before and after laser exposure, where as the corresponding ΔT

(°C) was calculated. In addition, experiments with lower laser powers were also performed. As shown in below Table 4.1, 3 different laser powers employed were 0.27, 0.53 and 1.02 W, while the exposure times for these powers were 420, 420 and 120 seconds respectively. It can be noticed in Table. 4.1, that for longer exposure times change in temperature ΔT (°C) was not significant at 0.27 and 0.53 W powers, whereas for power 1.02 W, there is further rise in the values of ΔT (°C) even with shorter exposure time.

Table 4.1 ΔT (°C) as a function of exposure time (sec) and power (W) in chicken breast sample study

Exposure Time (Sec)	Power (W)	Change in temperature (ΔT ° C)		
		1 mm	2 mm	3 mm
420 sec	0.27 W	1.5	1.25	1
420 sec	0.53 W	5.9	5.2	3.1
120 sec	1.02 W	16.1	9.75	5.82

On comparing with phantom study, similar trend was observed in the behavior of ΔT (°C) as a function of laser power for the same gold nanoshell concentration. However, ΔT (°C) in case of chicken breast sample were attained with longer laser exposure time (2 min) as compare to shorter exposure time (1 min) in point heat source phantom model. This may be due to the difference in physiology and optical properties of tissue sample and phantom model, which can affect the absorption of light. Another reason which may account in this discrepancy is rate of heat loss in the surrounding medium.

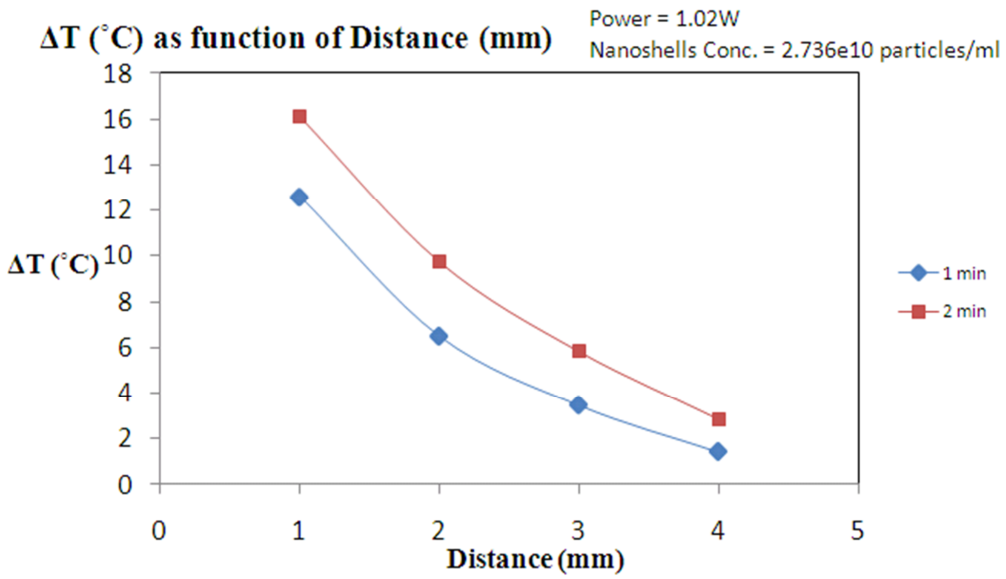

Figure 4.10 ΔT (°C) as a distance for exposure time 1 and 2 min, with nanoshell conc. 2.73e10 particles/ml and 1.02W power in chicken breast sample.

The above figure 4.10 shows change in temperature ΔT (°C) for 1 and 2 min exposure times. As discussed earlier in phantom studies, significant ΔT (~10 °C) observed was up to ~3mm, whereas for optimal setting of power and exposure time I observed similar heat spread pattern in this tissue sample study. Hence, ΔT (°C) observed in both the studies decays faster from the site of gold nanoshells injection i.e. where laser is illuminated. However, additional study on tissue sample may provide clearer picture for the experimental aspect on living animals. Furthermore, in order to check the effect of proposed method on living animal definitely some alterations are required in the protocol as I observed between phantom and tissue sample.

4.3 Rat study results

This section covers outcome for the animal study carried out with the aim to validate this proposed method. Therefore, an attempt was made to perform experiments on rats with prostate tumor in order to treat them. In this study, I have analyzed the data taken from two prostate cancer xenograft rat models, which involved direct injections of gold nanoshell suspensions into tumor sites and rapid heating of gold nanoshell embedded tumors, upon exposure to the near infrared light. Before any discussion on results, let's first see the basic idea which I aimed to employ for the thermal ablation treatment of particular size of tumors.

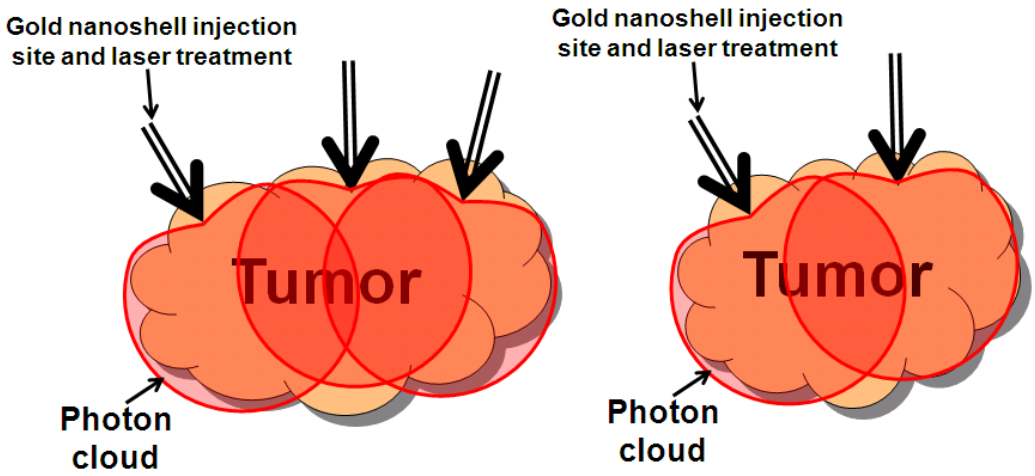

Figure 4.11 Schematic of the proposed technique for thermal ablation therapy of Tumors

Figure 4.11 illustrates two tumors with different sizes and their sites of laser treatment for hyperthermia. My plan is to cover tumor volume as a function of gold nanoshell injections and laser dosages. In figure 4.11, with the intention of demonstration, red colored shape shows NIR light pattern i.e. photon cloud in tumor. Overlapping of these photon cloud patterns would be advantageous as it might cover

total tumor volume. Previous studies on phantom and chicken breast tissue sample give me a rough idea of heat spread, which is significant to induce hyperthermia. Moreover, these studies also aid in determining parameters, such as gold nanoshell dosages and laser exposure time for a particular size of tumor. Figure 4.11 shows a comparison of two tumors with different sizes, their injection sites and laser treatment. A tumor with a larger size would require more number of gold nanoshell injections; in other words, an extra number of gold nanoshells need to be injected as compared to a smaller tumor. This can be explained, as I observed in point heat source phantom model and chicken breast tissue study, that single gold nanoshell injection would be useful to induce hyperthermia within a sphere of radius ~3mm. Therefore, I assume that to effectively treat a tumor of a larger size, more number of gold nanoshell injections would be required as shown in figure 4.11.

Two Copenhagen rats were used in this study. Each rat with two tumors on the back and with size ~1 cm was treated. Depending up on the size of tumor, gold nanoshell concentrations of 2.73×10^{10} particles/ml and 50µl volume were injected. After injections, a beam of laser at 800-µm through the coupled fiber was used to expose the gold nanoshells-embedded tumor by placing the fiber interstitially at a site of injection with ~1mm depth. Each injected site was delivered at 808 nm for 5 minutes. Temperature in the vicinity of the treatment area was monitored during laser activation, using thermocouple needle (Omega Technologies, Stamford, Connecticut). This was done to avoid overheating of the treatment site which may cause tissue carbonization.

Figure 4.12 Tumor volumes during the tumor growth period and after the treatment. In the graph, two rats are number as Rat1 and Rat2, whereas tumors on their back are grouped as T1 and T2. Also, both the tumors on Rat1 were given 3 injections of gold nanoshells; where as tumors on Rat2 were injected 2 gold nanoshell dosages. Treatment day for T2 and T1 on Rat1 and Rat2 was 7^{th} day, while T1 and T2 on Rat1 and Rat2 was 8^{th} day. It can be noticed from the trend of graph in figure 4.12 that even after treatment I still observe increase in tumor size. This is may be due to insufficient gold nanoshells dosages.

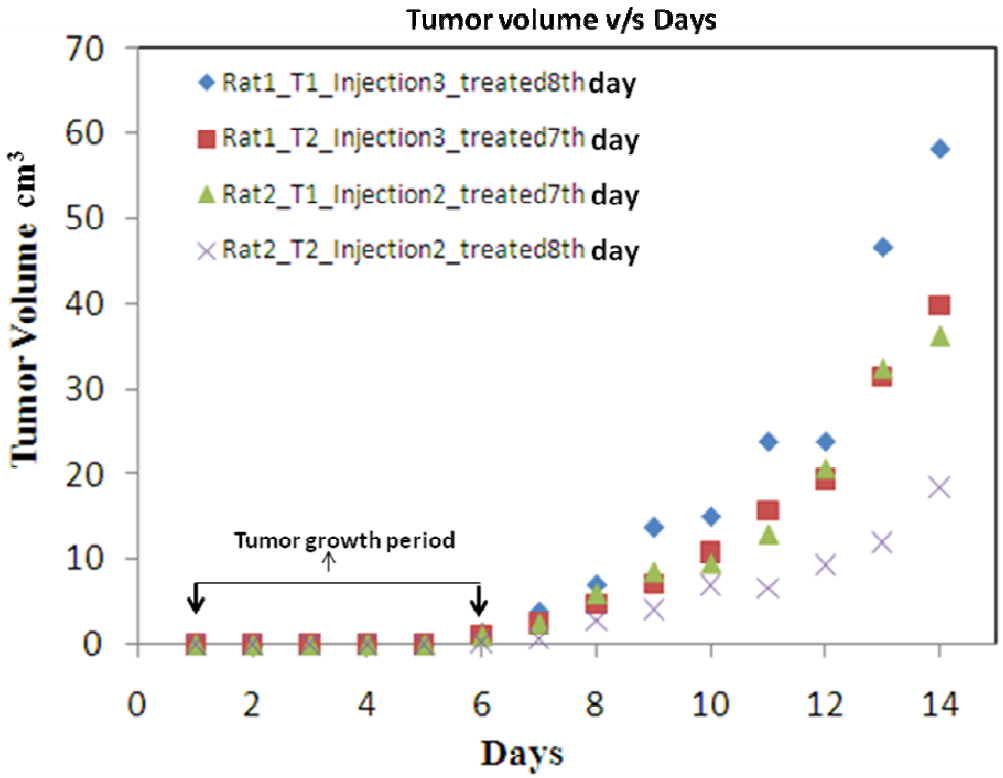

Figure 4.12 Graph shows Tumor volume as a function of days for 4 tumors, Rat1_T1, Rat1_T2, Rat2_T1, and Rat2_T2.

There are many others reasons which may account for this behavior of tumor growth. Tumors are highly vascularized in nature, i.e. they consist of a large number of blood vessels. This nature of tumor accounts for high absorption of light, and possible heat loss will occur due to continuous blood flow in vessels. Therefore, this may explain why I observed an increase in tumor size even after the treatment. However, the rate of tumor growth for the treated group needs to be compared with (untreated) control group. Further animal study with a large sample size is necessary in order to draw any meaningful conclusions.

CHAPTER 5

CONCLUSION AND FUTURE SCOPE

In my preliminary study, I explored gold nanoshells as NIR-sensitive heat absorbers to induce local hyperthermia to treat cancer. I observe that an increase in temperature at the maximum laser power was ~20% lower for layered heat source geometry than the point heat source geometry. Heat spread was significant ($\Delta T \geq 15°C$) up to ~3 mm from the site of laser treatment. From this exploratory study, I can conclude that the multiple gold nanoshell injections are beneficial over the conventional intravenous injection to increase the therapeutic efficacy. Moreover, I found that hyperthermia can be induced more efficiently by increasing laser exposure time without increasing dosage of gold nanoshell concentrations.

From the tissue phantom and chicken tissue studies, I conclude that heat spread was significant up to ~ 3 mm using the point heat source. The optimal relationship among laser powers, concentration of gold nanoshells and exposure time for real biological (chicken) tissue differs slightly as compared to the tissue phantom model. Hence, I could estimate parameter settings in the animal (rat) study by means of phantom and chicken tissue results. Moreover, temperature profiles would be helpful to estimate the number of gold nanoshell injections to effectively induce hyperthermia.

In the very preliminary rat study, I observed that even after the hyperthermia treatment there was an increase in size of tumors. Therefore, current study needs to be explored further with more animal experiments and by comparing the rate of tumor growth with untreated (control) rats. I have also planned to perform more animal measurements to validate the efficacy our methodology.

The match between the phantom experiments and chicken tissue study were found to be reasonable, having a similar trend but not having the exact readings. The reason for the exact match may be due to different physiology between the chicken tissue and phantom, in which surely have different optical properties. At the present, inefficacy observed in the animal study is unclear to me. Further investigations on the experimental parameters and their optimal relationships are needed to understand the inefficacy. For the future study, this project may be explored by further phantom experiments with more complex geometries and validation of the results using a larger animal sample size.

APPENDIX A

MATLAB SCRIPTS

MATLAB code for generating 3D plot

```
close all;
clear all;
clc;
% Load the data and extract the (x,y,z) information:
% load sample.mat

x=xlsread('data.xls','water','A2:A13');
y=xlsread('data.xls','water','B2:B13');
z1=xlsread('data.xls','water','C2:C13');
z2=xlsread('data.xls','water','D2:D13');
z3=xlsread('data.xls','water','E2:E13');
z4=xlsread('data.xls','water','F2:F13');

% Determine the minimum and the maximum x and y values:
xmin = min(x); ymin = min(y);
xmax = max(x); ymax = max(y);

% Define the resolution of the grid:
xres=100;
yres=100;

% Define the range and spacing of the x- and y-coordinates,
% and then fit them into X and Y
xv = linspace(xmin, xmax, xres);
yv = linspace(ymin, ymax, yres);
[Xinterp,Yinterp] = meshgrid(xv,yv);

% Calculate Z in the X-Y interpolation space, which is an
% evenly spaced grid:
% for i=1:4
%       if (i==1)
%       z1=i;
%    elseif (i==2)
%       z2=i;
%    elseif (i==3)
%       z3=i;
%    else (i==4)
%       z4=i;
%       end
Zinterp1 = griddata(x,y,z1,Xinterp,Yinterp);
Zinterp2 = griddata(x,y,z2,Xinterp,Yinterp);
```

```
Zinterp3 = griddata(x,y,z3,Xinterp,Yinterp);
Zinterp4 = griddata(x,y,z4,Xinterp,Yinterp);

% Generate the mesh plot
figure
% hold on;
mesh(Xinterp,Yinterp,Zinterp1), hold
mesh(Xinterp,Yinterp,Zinterp2)
mesh(Xinterp,Yinterp,Zinterp3)
mesh(Xinterp,Yinterp,Zinterp4)
colormap ('default')
xlabel Distance(mm); ylabel Power(W) ; zlabel('\deltaT(°C)');
legend('water','8.0e9','1.6e10','2.4e10');
% end
```

REFERENCES

[1] http://www.psa-rising.com/prostatecancer/prostate.htm

[2] http://www.mamashealth.com/organs/prostate.asp

[3] http://men.webmd.com/picture-of-the-prostate

[4] http://www.nebraskamed.com/ManageHealth/Libraries/Default.aspx?P=1257

[5] Website of Prostate Cancer: www.prostatecancercentre.co.uk/theprostate.html

[6] Website of Wikipedia: http://en.wikipedia.org/wiki/Prostate

[7] Website about Prostate Cancer: http://www.meb.uni-bonn.de/cancer.gov/CDR0000062965.html

[8] Website about prostate cancer http://www.prostate-cancer.com/

[9]http://www.cancer.org/docroot/cri/contect/cri_2_4_4x_androgen_suppression_hormone_therapy_36.asp

[10]Xiaohua Huang, Prashant K. Jain, Ivan H. El-Sayed, Mostafa A. El-Sayed, "Plasmonic photothermal therapy (PPTT) using gold nanoparticles", Springer-Verlag London Limited 2007, 3 August 2007

[11] W.R. Chen, R.L. Adams, R. Carubelli and R.E. Nordquist, "Laser-photosensitizer assisted immunotherapy: a novel modality for cancer treatment," *Cancer Letters* 115 (1997), pp. 25–30.

[12] D. Patrick O'Neal, Leon R. Hirsch, Naomi J. Halas, J. Donald Payne and Jennifer L. West, " Photo-thermal tumor ablation in mice using near infrared-absorbing nanoparticles**"** *Cancer Letters* 209(2004), pp. 171-176.

[13] Interstitial laser hyperthermia: a new approach to local destruction of tumours, A C Steger, W R Lees, K Walmsley, S G Bown

[14] Gurnani, P., “Near Infrared spectroscopic measurement of human and animal brain structures, in Bioengineering”, 2003, University of Texas at Arlington. p. 180.

[15] Joshua M. Stern, Jennifer Stanfield, Wareef Kabbani, Jer-Tsong Hsieh and Jeffrey A. Cadeddu, “Selective Prostate Cancer Thermal Ablation With Laser Activated Gold Nanoshells”, The Journal of Urology, 179(2008), pp. 748-753.

[16] http://www.nanoed.org/concepts_apps/AuNanoShells/InDepthIntroPg1.html

[17] http://www.trustingold.com/science/medical-uses/

[18] http://www.medicalnewstoday.com/articles/116660.php

[19] Gold nanoshells: Introduction and medical applications, Lynne M. Shenk, master of life science, 2007

[20]Gold nanoshells in biomedical application, Tim A. Erickson and James W. Tunnell

[21] Diagnostic and therapeutic applications of metal nanoshells by Leon Robert Hirsc, Rice University.

[22] Nanoshells assisted cancer therapy: Targeted Photothermal Tumor Ablation by Amanda Raley Lowery, Rice University.

[23] Suchita Kalele1, S. W. Gosavi1, J. Urban and S. K. Kulkarni, “Nanoshell particles: synthesis, properties and applications”.

[24] http://www.scholarpedia.org/article/Near_infrared_imaging

[25] http://www.nanoed.org/concepts_apps/AuNanoShells/InDepthIntroPg1.html

[26] Lars O. Svaasand, Charles J. Gomer, Elisa Morinelli, “On the Physical Rationale of Laser Induced Hyperthermia”.

[27] Website of Coherent Inc.: http://www.coherent.com/

[28] Website of Fluke: http://us.fluke.com/usen/Products/Hydra.htm

[29] Zhiyu Qian, Sundar S. Victor, Yueqing Gu, Cole A. Giller, Hanli Liu, ““Look-Ahead Distance” of a fiber probe used to assist neurosurgery: *Phantom and Monte Carlo study*”.

[30] Ali N. Bahadur, Cole A. Giller, Dheerendra Kashyap, Hanli Liu, “Determination of optical probe interrogation field of near-infrared reflectance: phantom and Monte Carlo study”.

[31] http://www.rxlist.com/cgi/generic/intralipid20.htm

[32]Review of tissue simulating phantoms for optical spectroscopy, imaging and dosimetry, Brian W. Pogue, Michael S. Patterson, Journal of Biomedical Optics 11_4_, 041102 July/August 2006.

BIOGRAPHICAL INFORMATION

Yajuvendra Rathore was born on May 5th, 1985 in Mahidpur, Madhya Pradesh, India. He graduated with a Bachelor's in Biomedical Engineering from Shri Govindram Seksaria Institute of Technology and Science (SGSITS) Engineering College, Rajiv Gandhi Proudyogiki Vishwavidyalaya University, India in April 2007. After that he joined the Master of Science program in Bioengineering at the University of Texas at Arlington in Fall 2007. He started working as a Graduate Research Assistant in Biomedical optics laboratory in November 2007. Apart from his current research on thermal ablation therapy for cancer; his interest also lies in Auto-fluorescence imaging, Time gated imaging, NIR spectroscopy and Designing and developing non-invasive tools for clinical applications.